J Am Soc Nephrol 15: 3083–3092, 2004

Expression and Function of Ets-1 during Experimental Acute Renal Failure in Rats

HIROYUKI TANAKA,* YOSHIO TERADA,* TAKAHIKO KOBAYASHI,* TOMOKAZU OKADO,* SEIJI INOSHITA,* MICHIO KUWAHARA,* ARUN SETH,† YASUFUMI SATO,‡ and SEI SASAKI*

**Homeostasis Medicine and Nephrology, Tokyo Medical and Dental University, Tokyo, Japan; †Department of Laboratory Medicine and Pathology, MRC Group in Periodontal Physiology, University of Toronto, Toronto, Ontario, Canada; and ‡Department of Vascular Biology, Institutes of Development, Aging and Cancer, Tohoku University, Sendai, Japan*

Abstract. The Ets family of transcription factors is defined by a conserved DNA-binding Ets domain that forms a winged helix-turn-helix structure motif. The Ets family is involved in a diverse array of biologic functions, including cellular growth, migration, and differentiation. The hypothesis in this study was that Ets-1 is re-expressed during regeneration after acute renal failure (ARF) and plays a key role in the transcriptional regulation of cyclin D1 and the cell cycle progression in renal tubular cells. For clarifying the significance of Ets-1 in ARF, a rat ARF model *in vivo* and LLC-PK1 cells as an *in vitro* model were used. After the left rat renal artery was clamped for 1 h, the whole kidney homogenate was examined and total RNA was extracted at 6, 12, 24, 48, and 72 h after reperfusion by Western blot analysis and real-time reverse transcription–PCR. Ets-1 mRNA and protein expression were strongly increased at 6 to 24 h after the ischemia, respectively. The expression of hypoxia-inducible factor-1α was increased dramatically as early as 6 h after ischemia-reperfusion and decreased at 48 and 72 h after ischemia-reperfusion. In the immunohistologic examination, Ets-1 was expressed in the proximal tubules and coexpressed with proliferating cell nuclear antigen (PCNA). Furthermore, overexpression of Ets-1 promoted the cell cycle and increased the promoter activity and protein expression of cyclin D1 in LLC-PK1 cells. Ets-1 promoter activity increased between 3 and 6 h in hypoxia, and hypoxia also induced changes in the Ets-1 protein level in LLC-PK1 cells. The Ets-1 induction by hypoxia was abolished by the transfection of dominant-negative hypoxia-inducible factor-1α. A gel shift assay demonstrated that Ets-1 binds to the ets-1 binding site of the cyclin D1 promoter in the ischemia-reperfusion condition. Overexpression of Ets-1 did not significantly change the caspase 3 activity or the value of cell death ELISA in LLC-PK1 cells. Taken together, these data suggest that Ets-1 plays a key role in the cell-cycle progression of renal tubules in ARF. The Ets-1 pathway may regulate the transcription of cyclin D1 and control the regeneration of renal tubules in ARF.

Ischemic acute renal failure (ARF) is the most common form of ARF in the adult population. The molecular basis of the events that lead to tubular regeneration after ARF is not understood (1–3). An understanding of the mechanisms that lead to renal cell proliferation and regeneration will be necessary for the exploration of novel therapeutic strategies for the treatment of ischemic ARF. It has been suggested that regeneration processes may recapitulate developmental processes to restore organ or tissue function (4,5). Adult tubular epithelial cells have a potent ability to regenerate after cellular damage. After ischemic renal damage, normally quiescent cells undergo dedifferentiation and acquire the ability to proliferate after their DNA synthesis is enhanced (6,7). In ARF, the regulation of cyclin and the cyclin-dependent kinase (CDK) inhibitor have been reported (8,9). The restriction point of the G1-to-S phase is determined by the activities of cyclin D1, cyclin A, cyclin E, and CDK (10,11). Cyclin D1 and cyclin A play key roles in the G1-S regulation of renal tubular epithelial cells (12).

The Ets family of transcription factors is defined by a conserved DNA-binding Ets domain that forms a winged helix-turn-helix structure motif (13,14). This family of transcription factors is involved in a diverse array of biologic functions, including cellular growth, migration, and differentiation (14–16). Ets-1 is the first member discovered in the Ets family of transcription factors. The expression of Ets-1 has been detected in various cells, and the roles of the Ets-1 gene expressed in mesodermal lineage cells, such as fibroblasts and endothelial cells, has drawn wide attention in the fields of embryogenesis and angiogenesis (17–20). During morphogenesis, Ets-1 expression occurs in vascular structures and branching tissues, including kidneys (18,21,22). In adult tissues, the levels of Ets-1 expression are much lower than in embryonic tissues, including the kidneys (18). Ets-1 expression has been reported in mesangial cells and to increase in the glomeruli and inter-

Received September 1, 2003. Accepted September 2, 2004.
Correspondence to Dr. Yoshio Terada, Homeostasis Medicine and Nephrology, Tokyo Medical and Dental University, 5-45, Yushima 1-chome, Bunkyo-ku, Tokyo 113-8519, Japan. Phone: 81-3-5803-5214; Fax: 81-3-5803-5215; E-mail: yterada.kid@tmd.ac.jp

1046-6673/1512-3083
Journal of the American Society of Nephrology

DOI: 10.1097/01.ASN.0000145459.54236.D3

stitium in rat crescentic glomerulonephritis (23,24). However, there have been no reports concerning Ets-1 expression during ARF. Recently, we and another group reported that the developmental genes Wnt-4 and Pax2 are expressed during ischemic acute renal injury and that Wnt-4 expression promotes the proliferation of renal tubular cells (25,26). These data suggested that some developmental genes are re-expressed during the recovery phase of ARF. A recent paper demonstrated that hypoxia induced Ets-1 expression *via* the activity of hypoxia-inducible factor-1 (HIF-1) in endothelial cells (27). Thus, there is a possibility that Ets-1, which is expressed during renal development, may play roles in ischemic renal failure.

Our hypothesis in this study is that Ets-1 is re-expressed during regeneration after ARF and plays a key role in the transcriptional regulation of cyclin D1 and in the cell-cycle progression in renal tubular cells. To test this hypothesis, we examined the expression pattern of Ets-1 during the recovery phase of an ischemia-reperfusion kidney. Our data demonstrate that Ets-1 is upregulated in the early phase of an ischemia-reperfusion kidney and that the overexpression of Ets-1, using an adenovirus, regulates the transcription of cyclin D1 and cell-cycle progression in renal tubular cells.

Materials and Methods

Cell Culture and Exposure to Hypoxia

LLC-PK1 cells, originally purchased from American Type Culture Collection (Rockville, MD), were grown in DMEM (Life Technologies, Gaithersburg, MD) supplemented with 50 IU/ml penicillin, 50 μg/ml streptomycin, and 10% heat-inactivated FCS (Life Technologies). Cells were cultured at 37°C in 20% O_2 and 5% CO_2 (referred to as the normoxic condition). For the hypoxia experiments, cells were placed in a hypoxic chamber (Bellow Glass, Vineland, NJ) that contained 0% O_2 and 5% CO_2, which was maintained at 37°C.

Plasmid Constructs

The Ets-1 reporter construct used for the luciferase assays contained a mouse Ets-1 promoter (−2.1 kbp) cloned upstream of the luciferase gene (28). The cyclin D1 reporter construct used for the luciferase assays contained a human cyclin D1 promoter from residues −944 to 139 cloned upstream of the luciferase gene (a gift of Dr. M. Eilers Zentrum für Molekularbiologie Heidelberg, Heidelberg, Germany) (29). Expression vectors coding for HIF-1α and dominant-negative (dn) HIF-1α were prepared as described previously (30,31) using the following primers: forward 5'-GGAAGACAACGCGGGCAC-3' and reverse 5'-GGAGCTGTGAATGTGCTGTGATCTGGC-3' and dnHIF-1α forward 5'-CCGCTCGAGACCATGCGAAGCAAAGAGTCTG-3' and reverse 5'-GGGGTACCTCACTTATCAAAAAGGCAGCT-3'. An open reading frame coding for the dnHIF-1α is a 1.1-kbp fragment whose product lacks both the DNA binding and transactivation domain. In both cases, RNA out of a C57BL mouse kidney was used as a template. The PCR fragment was subcloned into pcDNA3.1 (Invitrogen, San Diego, CA) and was processed to dideoxy-DNA sequencing.

Transient Transfection and Luciferase Assay

LLC-PK1 cells were transfected by the electroporation method with plasmid DNA (10 μg). Data are representative of at least four independent experiments performed in duplicate and are expressed as an n-fold increase in the luciferase activity calculated relative to the indicated level of Ets-1 promoter activity. Normalization was achieved by co-transfecting a β-galactosidase reporter construct, as described previously (12). Luciferase and β-galactosidase activities were measured according to the Promega (Madison, WI) protocol.

Recombinant Adenoviruses

Replication-defective, recombinant adenoviruses encoding human Ets-1 (Adets-1) and a control adenovirus (Adnull) were prepared as described previously (32). Replication-defective, recombinant adenoviruses encoding the rat dominant-negative Akt (AdAktDN) were also prepared as described previously (33). In this adenovirus, both Thr308 and Ser473 of the rat Akt1 were replaced by alanine (33).

Induction of ARF

Male Sprague-Dawley rats (Saitama Experimental Animal Supply, Saitama, Japan) that weighed 150 to 200 g were anesthetized intraperitoneally with sodium pentobarbital (30 mg/kg) at surgery. The left renal artery was occluded with Sugita aneurysm clips (Mizuho Ikakogyo, Tokyo, Japan) for 60 min. The clamps were removed after 60 min; the incisions were closed; and the rats were killed at 0, 6, 12, 24, 48, and 72 h ($n = 5$). The left kidney was removed quickly and processed for histologic evaluation, protein extraction, or RNA extraction. Age- and weight-matched Sprague-Dawley rats also received sham operations in a similar manner, except for clamping of the renal arteries at 6, 12, and 24 h ($n = 5$).

Isolation of Kidney Tissue and Histologic Examination

Rats were anesthetized with pentobarbital at indicated times after the ischemic event. Their kidneys were perfused with sterile PBS. The left kidney was excised quickly, frozen in liquid nitrogen, and homogenized in the SDS sample buffer described later.

For immunohistochemical studies, renal tissues were fixed in formalin overnight and then dehydrated and embedded in paraffin. Thin sections were examined with periodic acid-Schiff staining as described previously (34). Immunohistochemical staining was performed by a streptavidin and biotin technique using an anti–Ets-1–specific antibody (Santa Cruz Biochemical; N-276, cs-111), anti–proliferating cell nuclear antigen (PCNA)-specific antibody (Santa Cruz Biochemical; PC-10, cs-56), and anti–aquaporin-1–specific antibody (Santa Cruz Biochemical; B-11, sc-25287) as markers for proximal tubules, as described previously (35–37).

Western Blot Analysis

Homogenized total renal tissue or LLC-PK1 cells were lysed in an SDS sample buffer (50 mM HEPES [pH 7.5], 150 mM NaCl, 1.5 mM $MgCl_2$, 1 mM EGTA, 10% glycerol, 1% Triton X-100, 1 μg/ml aprotinin, 1 μg/ml leupeptin, 1 mM PMSF, and 0.1 mM sodium orthovanadate) at 4°C (38). Protein was transferred to a nitrocellulose membrane and probed with the anti–Ets-1–specific antibody. The primary antibodies were detected using horseradish peroxidase–conjugated rabbit anti-mouse IgG and visualized by the Amersham ECL system (Amersham, Arlington Heights, IL).

Electrophoretic Mobility Shift Assay

Nuclear extracts from the renal cortex were prepared as described previously (39). The extracts (10 μg) underwent a reaction in a premixed incubation buffer (Gel Shift Assay Kit; Promega) with the γ-^{32}P-end-labeled ets-1 binding site of a cyclin D1 promoter-lesion (5'-GATCTCGAGCAGGAAGTTCGA-3') for 30 min at 25°C. To establish the specificity of the reaction, we performed competition

assays with 100-fold excess of unlabeled ets-1 binding oligonucleotides (heterologous competitor DNA). To perform supershift assay, we added 5 μg of anti–Ets-1 antibody (Santa Cruz; N-276, cs-111) to the nuclear extracts, incubated extracts for 1 h at 4°C, and performed gel shift assay. After the reaction, the samples were analyzed on a 6% nondenaturing polyacrylamide gel. The gel was dried, and the protein-DNA complexes were visualized by autoradiography.

Real-Time Quantitative PCR

We performed a reverse transcription–PCR (RT-PCR) reaction for Ets-1 from RNA extracted from the ischemia-reperfusion kidneys. Total RNA was harvested from renal tissue using TRI-REAGENT (Life Technologies) (40). One microgram of total RNA samples was used for the RT-PCR as follows. The real-time quantitative PCR method was used to detect accurately the changes in Ets-1 gene copies. Total RNA was harvested from renal tissue. Rat Ets-1 and glyceraldehyde-3-phosphate-dehydrogenase (GAPDH) mRNA were amplified. The primers for rat Ets-1 were 5'-GCCCAGCTTCATCACAGAGT-3' (upper) and 5'-TGTTGAAAGATGACTGGCTG-3' (lower) (23). The predominant cDNA amplification product was predicted to be 296 bp in length. The RT-PCR of GAPDH served as positive controls. The primers for rat GAPDH were 5'-TCCCTCAAGATTGTCAGCAA-3' (upper) and 5'-AGATCCACAACGGATACATT-3' (lower) (41). The predominant cDNA amplification product was predicted to be 309 bp in length. PCR products were detected and quantified in real time using the LightCycler Real-Time PCR (Roche Molecular Biochemicals, Tokyo, Japan) as described previously (42,43). A three-step PCR was performed for 35 cycles. Denaturation was performed at 94°C for 20 s, annealing at 55°C for 20 s, and extension at 72°C for 30 s. The PCR products of Ets-1 and GAPDH were subcloned to the TA cloning vector (Promega, Biotec, Madison, WI) as described previously (40). The plasmids that contained Ets-1 cDNA and GAPDH cDNA were used to make standard curves of quantitative PCR.

Cell Proliferation Analysis by [^{3}H]Thymidine Incorporation

After transfection, the LLC-PK1 cells were plated in 24-well plates and incubated in a medium without FCS for 20 h. For the last 4 h, the cells were pulsed with 1 μCi [^{3}H]thymidine (Amersham). After the incubation, the cells were redissolved in 0.5 M NaOH and counted in an Aquasol-2 scintillation cocktail (NEN Research Products, Boston, MA) (44).

Caspase 3 Assays

A Caspase 3 Fluorometric Protease Assay Kit (MBL, Tokyo, Japan) was used for the measurement of caspase 3 activities as described previously (33). In brief, the cells were plated in six-well dishes and infected with adenoviruses. The cell lysates then were incubated with the same amounts of reaction buffer and a 50-mM DEVD-AFC substrate for 2 h at 37°C. Fluorescence was monitored with an excitation wavelength of 400 nm and an emission wavelength of 505 nm.

Cell Death ELISA

Histone-associated DNA fragments were quantified by ELISA (Boehringer Mannheim). All cells from each well were collected by trypsinization and pipetting, then pelleted (800 rpm, 5 min), lysed, and subjected to ELISA capture according to the manufacturer's protocol (33). Cytosolic proteins were collected using a cell lysis buffer and centrifuged according to the manufacturer's protocol. The nucleus formed into a pellet, and the cytoplasmic fraction became the supernatant. These supernatants were collected for the ELISA assay. Each experiment was carried out in triplicate and repeated in at least five independent experiments.

Statistical Analyses

The results are given as means ± SEM. The differences were tested using a two-way ANOVA followed by the Scheffe test for multiple comparisons. Two groups were compared by the unpaired *t* test. $P < 0.05$ was considered significant.

Results

Western Blot Analysis of the Protein Expression of Ets-1 and HIF-1α after Ischemic Renal Failure

The left renal artery was clamped for 60 min and the left kidney was excised at 0, 6, 12, 24, 48, and 72 h after reperfusion. Western blot analysis was used to detect the protein levels of Ets-1 and actin. The expression of Ets-1 was weak in the control kidney (0 h) and sham-operated kidneys (6 and 12 h; Figure 1). The expression of Ets-1 was dramatically increased at 6 to 24 h after ischemia-reperfusion (Figure 1A). The upregulation of Ets-1 protein expression was temporary, with the intensity of the Ets-1 band decreasing at 48 and 72 h after ischemia-reperfusion. The protein levels of Ets-1 exhibited no changes after 6 to 12 h in the sham-operated rats (the data of 24 h are not shown). Western blot analysis was used to detect the protein levels of HIF-1α and actin. The expression of HIF-1α was weak in the control kidney (0 h) and sham-operated kidneys (6 and 12 h; Figure 1). The expression of HIF-1α was dramatically increased as early as 6 h after ischemia-reperfusion (Figure 1A). The upregulation of HIF-1α protein expression was temporary, with the intensity of the

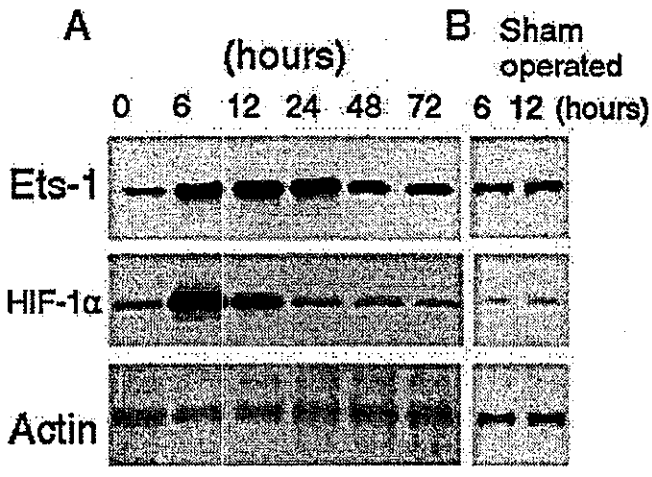

Figure 1. Protein expressions of Ets-1 and hypoxia-inducible factor-1α (HIF-1α) in the kidneys of rats that were subjected to 60 min of renal ischemia. The left renal artery was clamped for 60 min, and the left kidney was excised at 0, 6, 12, 24, 48, and 72 h after reperfusion (A). A sham operation was performed, and the left kidney was excised at 6 and 12 h (B). Extracted protein (20 μg) from renal tissue was separated by SDS-PAGE gels. Ets-1, HIF-1α, and actin protein levels were detected by Western blot analysis.

Ets-1 band decreasing at 48 and 72 h after ischemia-reperfusion. We performed an immunoblot for actin as a loading marker, and there were no significant changes in actin during ischemia-reperfusion. The protein levels of HIF-1α exhibited no changes after 6 to 12 h in the sham-operated rats (the data of 24 h are not shown).

Immunohistochemical Examination of Ets-1 in ARF

Next, we performed immunohistologic studies on Ets-1 in ARF (Figures 2 and 3). In a low-power view examination, Ets-1 expression was observed in cortical renal tubules at 12 h after ischemia-reperfusion (Figure 2A). We used the anti–aquaporin-1 antibody as a marker of proximal tubules (35–37). As shown in Figure 2, A and B, the expression of Ets-1 is co-localized with aquaporin-1 in the low-power view examination in continuous sections. Conversely, only a slight Ets-1 expression is observed in the renal cortex form control rats (Figure 2E), whereas the expression of aquaporin-1 is clearly observed in the renal cortex form control rats (Figure 2F). From these results, Ets-1 was expressed mainly in the proximal tubules of the renal cortex 12 h after ischemia-reperfusion (Figure 2). In the renal medulla, Ets-1 could not be detected in either the ischemia-reperfusion kidney (Figure 2C) or the control kidney (data not shown). In a higher-power view, Ets-1 staining was observed in the nucleus of proximal tubular cells (Figure 3A). As shown in Figure 3B, the expression of Ets-1 is co-localized with aquaporin-1 in continuous sections. To examine the specificity of the antibody, we used a blocking peptide (sc-111p; Santa Cruz Biotechnology). The nuclear signal diminished in the presence of the blocking peptide in the cortex of ischemia-reperfusion kidney (Figures 2G and 3C).

To co-localize Ets-1 with dividing cells, we examined Ets-1 staining at 24 h after ischemia-reperfusion (Figure 4). Ets-1 expression was observed at the proximal tubules of the cortex (Figure 4, A and C). PCNA staining was also observed at the proximal tubules of the cortex (Figure 4, B and D). The higher power view of Ets-1 staining also revealed co-localization of Ets-1 and PCNA in the same tubules at 24 h after ischemia-reperfusion in continuous sections (Figure 4, C and D). Conversely, only a slight Ets-1 expression is observed in the renal cortex from control rats (Figure 4E). No PCNA-positive tubules were observed from control rats (Figure 4F). To examine the specificity of the antibody, we used a blocking peptide (sc-9857p; Santa Cruz Biotechnology). The nuclear signal diminished in the presence of the blocking peptide in the cortex of ischemia-reperfusion kidney (Figure 4G).

Real-Time PCR

Quantification of the Ets-1 mRNA transcript using the real-time quantitative PCR method revealed 8.0-fold (6 h), 3.8-fold (12 h), and 2.2-fold (24 h) increases in Ets-1 mRNA levels compared with the 0-h value (Figure 5). The linear curve between the cDNA amount and PCR product was observed in the same range utilized by using the Ets-1 cDNA plasmid. The signals of Ets-1 were not significantly changed in the sham-operated rat kidneys. The GAPDH signal was not significantly changed by ischemia-reperfusion (Figure 5A).

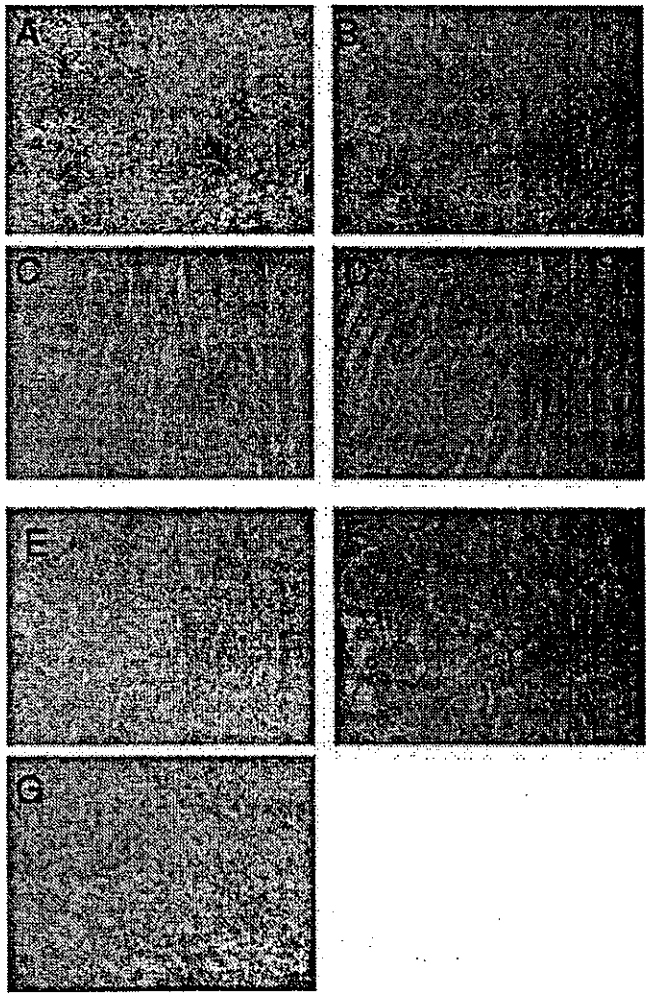

Figure 2. Immunohistological examination of Ets-1 in ischemic-reperfusion kidneys. Immunohistochemical analyses at a low-power view (×100) of the renal cortex were performed with antibodies against Ets-1 (A) and aquaporin-1 (B) at 12 h after ischemic injury. Immunohistochemical analyses at a low-power view (×100) of the renal medulla were performed with antibodies against Ets-1 (C) and aquaporin-1 (D) at 12 h after ischemic injury. Immunohistochemical analyses at a low-power view (×100) of the renal cortex of control kidneys were performed with antibodies against Ets-1 (E) and aquaporin-1 (F). Immunohistochemical analyses at a low-power view (×100) of the renal cortex of ischemic kidneys were performed with antibodies against Ets-1 in the presence of a blocking peptide (G). Histologic examinations A and B, C and D, and E and F are continuous sections, respectively.

Hypoxia Stimulates Ets-1 Expression and Promoter Activity via HIF-1α in LLC-PK1 Cells

To examine whether hypoxia-reperfusion stimulates Ets-1 expression and promoter activity in renal tubular cells, we used a hypoxic culture system with LLC-PK1 cells. We exposed LLC-PK1 cells to hypoxia for 3, 6, and 6 h + reoxygenation 6 h and examined the promoter activity of Ets-1 and the expression of Ets-1 protein by Western blot analysis. In the

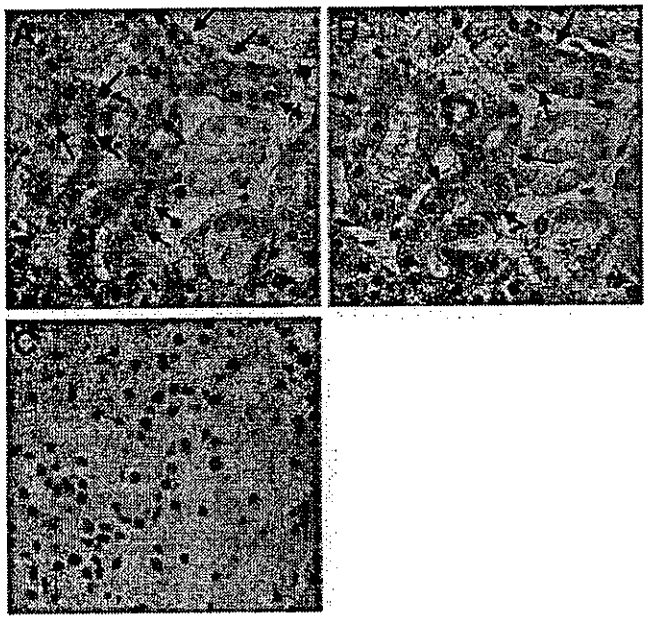

Figure 3. Immunohistologic examination of Ets-1 in proximal tubules of ischemic-reperfusion kidneys. Immunohistochemical analyses at a high-power view (×400) of the renal cortex were performed with antibodies against Ets-1 (A) and aquaporin-1 (B) at 12 h after ischemic injury. Histologic examinations A and B are continuous sections. The arrows indicate Ets-1– and aquaporin-1–positive cells. When a blocking peptide was added to the anti–Ets-1 antibody solution, no positive signal was observed in ischemia-reperfusion kidney (12 h; C).

promoter assay experiments, the Ets-1 promoter-luciferase plasmid was transfected in LLC-PK1 cells 48 h before hypoxia. As shown in Figure 6B, Ets-1 promoter activity was increased 7.1-fold at 3 h, 9.1-fold at 6 h, and 12.1-fold at 6 h + reoxygenation 6 h. Hypoxia also induced changes in the Ets-1 protein level in LLC-PK1 cells (Figure 6A). There were no significant changes in actin during hypoxia/reoxygenation.

To test whether the upregulation of Ets-1 is dependent of HIF-1α, we examined Ets-1 protein expression and promoter activity in HIF-1α–transfected LLC-PK1 cells and dnHIF-1α–transfected LLC-PK1 cells. The hypoxic inducibility of the Ets-1 promoter assay in HIF-1α–overexpressing and dnHIF-1α–overexpressing cells was 17.8- and 1.5-fold, respectively, as compared with 9.1-fold in control LLC-PK1 cells at 6 h (Figure 6D). The Western blot analysis demonstrated that transfection of dnHIF-1α reduced the increment of Ets-1 protein by hypoxia (Figure 6C). These results indicated that the upregulation of Ets-1 by hypoxia is dependent on HIF-1α.

Electrophoretic Mobility Shift Assay

To examine the induction of cyclin D1 expression *via* the ets-1 binding site, we performed an electrophoretic mobility shift assay using nuclear extracts from a rat renal cortex. Figure 7 shows that the nuclear extract from the ischemia-reperfusion rat renal cortex gave rise to a protein-DNA complex (Figure 7, lane 2). However, we did not detect protein-DNA complex band in control rat renal cortex (Figure 7, lane 3). The band was completed using 100-fold excess of the unlabeled oligonucleotides (heterologous competitor DNA; Figure 7, lane 4). When nuclear extracts from the ischemia-reperfusion rat renal cortex were preincubated with anti–Ets-1 antibody, the super-

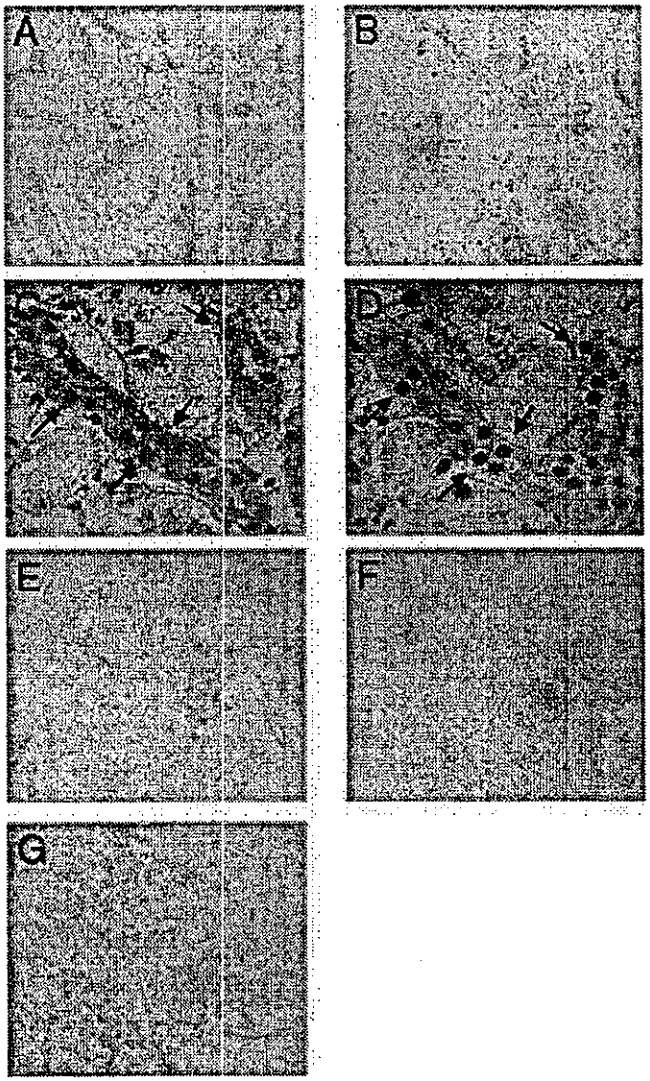

Figure 4. Immunohistologic co-localization of Ets-1 and proliferating cell nuclear antigen (PCNA) in the proximal tubules of ischemic-reperfusion kidneys. Immunohistochemical analyses at a low-power view (×100) of the renal cortex were performed with antibodies against Ets-1 (A) and PCNA (B) at 24 h after ischemic injury. Histologic examinations A and B are continuous sections. Immunohistochemical analyses at a high-power view (×400) of the renal cortex of ischemic kidneys were performed with antibodies against Ets-1 (C) and PCNA (D) at 24 h after ischemic injury. The arrows indicate Ets-1– and PCNA-positive cells. Immunohistochemical analyses at a low-power view (×100) of the renal cortex were performed with antibodies against Ets-1 (E) and PCNA (F) of control kidney. Histologic examinations E and F are continuous sections. When a blocking peptide was added to the anti-PCNA antibody solution, no positive signal was observed in ischemia-reperfusion kidney (12 h; G).

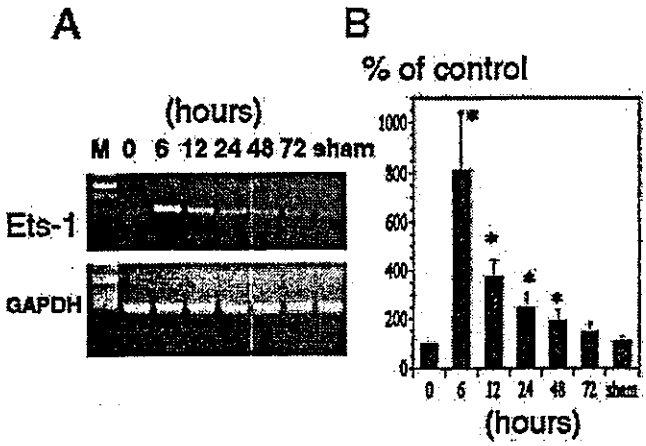

Figure 5. Quantitative analysis of Ets-1 expression in ischemic-reperfusion kidneys using real-time PCR. The left renal arteries were clamped for 60 min, and kidneys were excised at 0, 6, 12, 24, 48, and 72 h after reperfusion. Sham-operated rats at 6 h were also examined. Extracted total RNA were subjected to quantitative PCR using the LightCycler Real-Time PCR for the estimation of relative Ets-1 mRNA levels and the Ets-1 to glyceraldehyde-3-phosphate-dehydrogenase (GAPDH) mRNA ratio, as described in the Materials and Methods section. (A) The representative agarose gels for Ets-1 and GAPDH are shown. (B) Each column with a bar shows the mean ± SEM ($n = 5$). *$P < 0.05$ *versus* control rats.

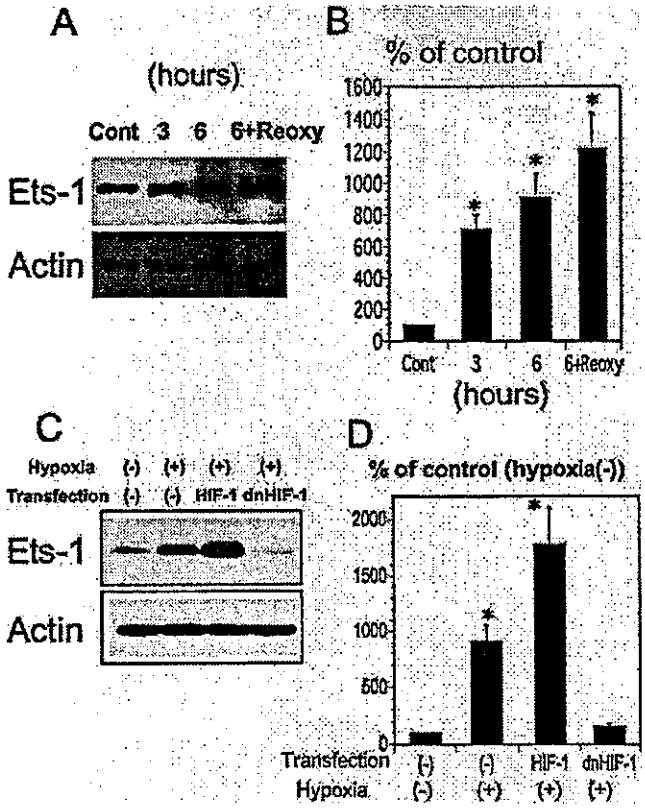

Figure 6. Hypoxia stimulates Ets-1 expression and promoter activity *via* HIF-1α in LLC-PK1 cells. To examine whether hypoxia/reoxygenation stimulates Ets-1 expression and promoter activity in renal tubular cells, we used a hypoxic culture system with LLC-PK1 cells. We exposed LLC-PK1 cells to hypoxia for 3, 6, and 6 h + reoxygenation 6 h and examined the promoter activity of Ets-1 and the expression of Ets-1 protein by Western blot analysis. (A) Hypoxia induced changes in the Ets-1 protein level in LLC-PK1 cells by Western blot analysis. (B) Ets-1 promoter activity was increased 7.1-fold at 3 h, 9.1-fold at 6 h, and 12.2-fold at 6 h + reoxygenation. (C and D) To test whether the upregulation of Ets-1 is dependent on HIF-1α, we examined Ets-1 protein expression and promoter activity in HIF-1α–transfected LLC-PK1 cells and dnHIF-1α–transfected LLC-PK1 cells; $n = 5$, mean ± SEM; *$P < 0.05$ *versus* control.

shift of the band was observed (Figure 7, lane 6). These results confirm that Ets-1 binds to the ets-1 binding site of the cyclin D1 promoter in the ischemia-reperfusion condition.

Cell Proliferation and Cyclin D1 Expression by the Overexpression of Ets-1 in LLC-PK1 Cells

We first examined the effects of the overexpression of Ets-1, using an adenovirus, on the cell proliferation of LLC-PK1 cells by [^{3}H]thymidine uptake. Figure 8A shows the effects of Ets-1 on [^{3}H]thymidine uptake. Overexpression of Ets-1 stimulated the [^{3}H]thymidine uptake to 225% dose-dependently. Overexpression of Adnull (control adenovirus) did not significantly change the [^{3}H]thymidine uptake in LLC-PK1 cells. We next examined the role of Ets-1 in the regulation of cyclin D1 promoter activity and protein expression. We performed a transient transfection with the cyclin D1-luciferase reporter gene and the β-galactosidase expression vector and then infected it with Adets-1 or Adnull. When Ets-1 was overexpressed, cyclin D1 promoter activity increased significantly, by 3.6-fold, in LLC-PK1 cells. In the case of transfection of Adnull, there were no significant changes in cyclin D1 promoter activity or protein expression (Figure 8B). When Adets-1 was transfected, a higher level of cyclin D1 protein expression could be detected when compared with Adnull (Figure 8B).

Apoptotic Changes by the Overexpression of Ets-1 in LLC-PK1 Cells

In vascular endothelial cells, overexpression of Ets-1 causes apoptotic changes (30). Thus, we examined the effects of the overexpression of Ets-1 using an adenovirus on apoptotic changes of LLC-PK1 cells by caspase 3 activity and a cell death ELISA kit. We used AdAktDN as a positive control. Overexpression of AdAktDN caused apoptotic changes in renal tubular cells (33). Figure 9 shows the effects of Adets-1, AdAktDN, and Adnull on caspase 3 activity and the cell death ELISA. Overexpression of AdAktDN stimulated caspase 3 activity and the value of cell death ELISA. Overexpression of Adets-1 did not significantly change stimulated caspase 3 activity or the value of cell death ELISA in LLC-PK1 cells. These data demonstrated that Ets-1 does not cause apoptotic changes in LLC-PK1 cells.

Discussion

In the present study, we demonstrated that Ets-1 is upregulated in proximal tubules in the recovery phase of ARF, that

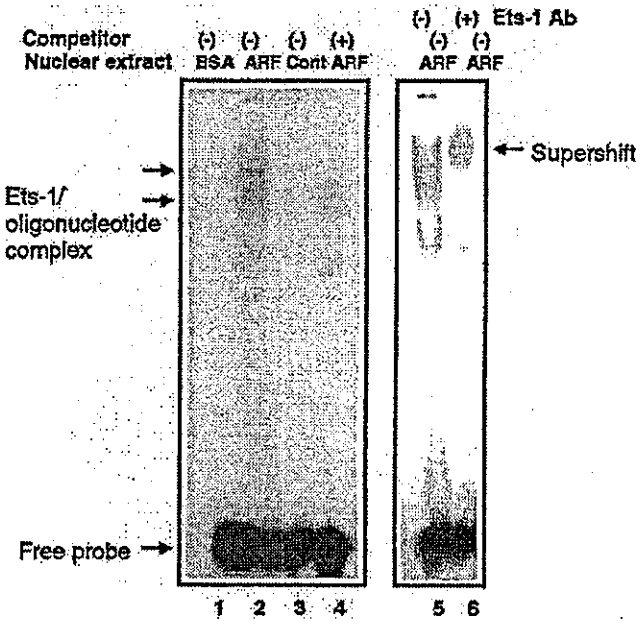

Figure 7. Electrophoretic mobility shift assay detected a protein binding to the promoter sequence of cyclin D1 in the nuclear extract of an ischemia-reperfusion rat kidney. A nuclear extract from renal cortex was prepared form the cortex of an ischemia-reperfusion rat kidney and a control rat kidney. The nuclear extract (10 μg) underwent a reaction in a premixed incubation buffer (gel shift assay kit) with a γ-^{32}P-end-labeled Ets-1 binding site of the cyclin D1 promoter lesion (5'-GATCTCGAGCAGGAAGTTCGA-3') for 30 min at 25°C. To establish the specificity of the reaction, we performed competition assays with 100-fold excess of unlabeled ets-1 biding oligonucleotides (heterologous competitor DNA). To perform supershift assay, we added 5 μg of anti–Ets-1 antibody (N-276, cs-111) to the nuclear extracts, incubated the extracts for 1 h at 4°C, and performed gel shift assay. Negative control without nuclear extract (lane 1), nuclear extract of ischemia-reperfusion kidney (lane 2), nuclear extract of control kidney (lane 3), and nuclear extract of ischemia-reperfusion kidney with 100-fold excess of unlabeled oligonucleotide (heterologous competitor DNA; lane 4) are shown. Nuclear extract of ischemia-reperfusion kidney incubated without anti–Ets-1 antibody (lane 5) and nuclear extract of ischemia-reperfusion kidney incubated with anti–Ets-1 (lane 6, supershift) are shown.

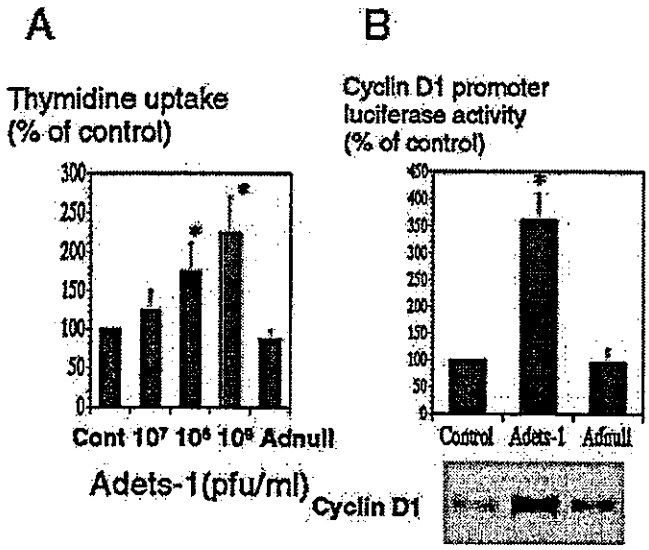

Figure 8. Cell proliferation and cyclin D1 expression by the overexpression of Ets-1 in LLC-PK1 cells. (A) We examined the effects of the overexpression of Ets-1 using an adenovirus on the cell proliferation of LLC-PK1 cells by [^{3}H]thymidine uptake. A shows the effects of Ets-1 on [^{3}H]thymidine uptake. (B) We next examined the role of Ets-1 in the regulation of cyclin D1 promoter activity and protein expression. We performed a transient transfection with the cyclin D1-luciferase reporter gene and the β-galactosidase expression vector and then infected it with either Adets-1 or Adnull (10^9 pfu/ml). When Ets-1 was overexpressed, cyclin D1 promoter activity increased significantly, by 3.6-fold, in LLC-PK1 cells; $n = 5$, mean ± SEM; $^*P <$ 0.05 *versus* control.

hypoxia causes the transcriptional stimulation of Ets-1 in LLC-PK1 cells *via* HIF-1α, and that the overexpression of Ets-1 stimulates [^{3}H]thymidine uptake and cyclin D1 transcription in renal tubular cells.

Recovery from ARF requires the replacement of damaged cells with new cells that restore tubule epithelial integrity. Regeneration processes are characterized by the proliferation of dedifferentiated cells and subsequent redifferentiation of the daughter cells into the required cell phenotype. A similar phenomenon can also be observed during embryogenesis. Therefore, it was postulated that regeneration processes may repeat parts of the genetic program that serve during organogenesis to reestablish proper tissue function after damage (5,45). Recently, we reported that the developmental gene Wnt-4 is expressed in ischemic acute renal injuries and that Wnt-4 expression promotes the proliferation of renal tubular cells (26). This article suggested that some developmental genes are re-expressed during recovery of ARF. To confirm this hypothesis, we examined the expression patterns and function of Ets-1 in an ischemic acute renal model and in renal tubular cells.

In this study, we first demonstrated that Ets-1 expression is upregulated in the early phase of ischemic ARF. The Ets-1 expression was localized exclusively in the proximal tubule at the site of tubule regeneration where PCNA is expressed. These results suggest that Ets-1 protein may induce the transformation of regenerative renal tubular cells. During development, Ets-1 expression occurs in vascular structures and branching tissues, including the kidneys (18). In the adult kidney, the levels of Ets-1 expression are much lower than in the embryonic kidney (18,22). Thus, our data suggest that the cells that express Ets-1 after ischemic injury have characteristics of embryonic renal cells, such as in the mesenchymal-to-epithelial progression and proliferation.

Our data also indicate for the first time that Ets-1 signaling contributes to the activation of cyclin D1 promoter and protein expression. Sequences that resemble the core motif (GGA) required for Ets protein binding are located within the proximal cyclin D1 promoter (16). Overexpression of Ets-2 activates the

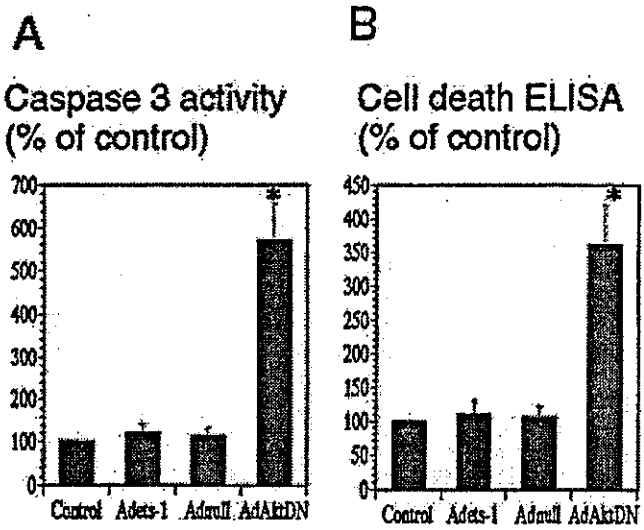

Figure 9. Apoptotic changes were not observed by the overexpression of Ets-1 in LLC-PK1 cells. We examined the effects of the overexpression of Ets-1 using an adenovirus on apoptotic changes of LLC-PK1 cells by caspase 3 activity and a cell death ELISA kit. AdAktDN was used as a positive control. Overexpression of AdAktDN stimulated caspase 3 activity (A) and the value of cell death ELISA (B). Overexpression of Adets-1 did not significantly change stimulated caspase 3 activity (A) or the value of cell death ELISA (B) in LLC-PK1 cells; $n = 5$, mean ± SEM; $^*P < 0.001$ *versus* control.

cyclin D1 promoter through the proximal 22 bp (46). The Ets-1 pathway plays a key role in normal embryonic development and in malignant vascular formation (17–20). However, the functional role of the Ets-1 signaling pathway in renal tubular cells is not well known. Our data demonstrate that overexpression of Ets-1 increases cyclin D1 promoter activity, protein expression, and cell-cycle progression in renal epithelial cells. If this is the case, then the expression of Ets-1 in the recovery phase of ARF could be expected to promote cell-cycle progression after tubular injury. Our data also demonstrated that the Ets-1 binding site of the cyclin D1 promoter binds to the nuclear extract of ischemic renal tissue. Our ischemia-reperfusion model also demonstrated that Ets-1 was co-localized with PCNA, suggesting that Ets-1 might be a proliferative signal in regenerating renal tubules.

In vascular endothelial cells, overexpression of Ets-1 caused apoptotic changes (32). Apoptosis of renal tubular cells is observed during ARF (47,48). Thus, we hypothesized that upregulated Ets-1 may cause apoptotic changes in renal tubular cells. To demonstrate this, we examined the effects of the overexpression of Ets-1 on apoptotic changes in LLC-PK1 cells. AdAktDN was used as a positive control, and overexpression of AdAktDN caused apoptotic changes in LLC-PK1 cells as shown in Figure 6. However, in our experimental conditions, the overexpression of Adets-1 did not significantly change caspase 3 activity or the value of cell death ELISA in LLC-PK1 cells. This result suggests that the apoptotic phenomenon caused by Ets-1 may be dependent on cell types or tissues. In the case of renal tubular cells, Ets-1 does not seem to play a role in apoptosis in ARF.

We have yet to see which kinds of mechanisms induce the transient upregulation of Ets-1 after ischemia-reperfusion acute renal injury. A recent paper by Oikawa *et al.* (27) reported that hypoxia induced Ets-1 *via* the activity of HIF-1α. In their study, the Ets-1 promoter contained a hypoxia-responsive element-like sequence, and HIF-1α bound to it under the hypoxic condition. The expression of HIF-1α was dramatically increased as early as 6 h after ischemia-reperfusion (Figure 1C). The upregulation of HIF-1α protein expression was temporary; the intensity of the Ets-1 band decreased at 48 and 72 h after ischemia-reperfusion. The time course of HIF-1α exceeded the time course of Ets-1. The hypoxic inducibility of the Ets-1 promoter assay is inhibited by the overexpression of dnHIF-1α in LLC-PK1 cells. The Western blot analysis also demonstrated that transfection of dnHIF-1α reduced the increase of Ets-1 protein by hypoxia (Figure 6C). These results indicated that the upregulation of Ets-1 by hypoxia is dependent on HIF-1α. This evidence led to the hypothesis that ischemia causes hypoxia in the renal tubule, and the hypoxic condition induces HIF-1α, then HIF-1α activates Ets-1 transcription in renal tubular cells. It will be of interest to examine which kinds of signal cascades exist between ischemia and Ets-1 induction. Further studies will be necessary to gain a more precise understanding of the molecular mechanisms of renal recovery after ischemia-reperfusion injury.

Acknowledgments

An abstract of this work was presented at the 2003 Annual Meeting of the American Society of Nephrology, November 12–17, 2003, San Diego, CA.

We thank Dr. M. Eilers for providing the cyclin D1-promoter plasmid.

References

1. Molitoris BA: Ischemic acute renal failure: Exciting times at our fingertips. *Curr Opin Nephrol Hypertens* 7: 405–406, 1998
2. Bonventre JV: Mechanisms of ischemic acute renal failure. *Kidney Int* 43: 1160–1178, 1993
3. Safirstein R, DiMari J, Megyesi J, Price P: Mechanisms of renal repair and survival following acute injury. *Semin Nephrol* 18: 519–522, 1998
4. Bacallao R, Fine LG: Molecular events in the organization of renal tubular epithelium: From nephrogenesis to regeneration. *Am J Physiol* 257: F919–F924, 1989
5. Wallin A, Zhang G, Jones TW, Jaken S, Stevens JL: Mechanism of the nephrogenic repair response. Studies on proliferation and vimentin expression after 35S-1,2-dichlorovinyl-L-cysteine nephrotoxicity in vivo and in cultured proximal tubule epithelial cells. *Lab Invest* 66: 474–484, 1992
6. Witzgall R, Brown D, Schwarz C, Bonventre JV: Localization of proliferating cell nuclear antigen, vimentin, c-fos, and clusterin in the postischemic kidney. *J Clin Invest* 93: 2175–2188, 1994
7. Safirstein R: Gene expression in nephrotoxic and ischemic acute renal failure. *J Am Soc Nephrol* 4: 1387–1395, 1994
8. Megyesi J, Udvarhelyi N, Safirstein RL, Price PM: The p53-independent activation of transcription of p21 WAF1/CIP1/SDI1 after acute renal failure. *Am J Physiol* 270: F1211–F1216, 1996

9. Megyesi J, Safirstein RL, Price PM: Induction of p21WAF1/CIP1/SDI1 in kidney tubule cells affects the course of cisplatin-induced acute renal failure. *J Clin Invest* 101: 777–782, 1998
10. Kato J, Matsushime H, Hiebert SW, Ewen ME, Sherr CJ: Direct binding of cyclin D to the retinoblastoma gene product (pRb) and pRb phosphorylation by the cyclin D-dependent kinase CDK4. *Genes Dev* 7: 331–342, 1993
11. Sherr CJ, Kato J, Quelle DE, Matsuoka M, Roussel MF: D-type cyclins and their cyclin-dependent kinases: G1 phase integrators of the mitogenic response. *Cold Spring Harb Symp Quant Biol* 59: 11–19, 1994
12. Terada Y, Nakashima O, Inoshita S, Kuwahara M, Sasaki S, Marumo F: TGF-beta-activating kinase-1 inhibits cell cycle and expression of cyclin D1 and A in LLC-PK1 cells. *Kidney Int* 56: 1378–1390, 1999
13. Laudet V, Hanni C, Stehelin D, Duterque CM: Molecular phylogeny of the ETS gene family. *Oncogene* 18: 1351–1359, 1999
14. Sharrocks AD: The ET: S-domain transcription factor family. *Nat Rev Mol Cell Biol* 2: 827–837, 2001
15. Sharrocks AD, Brown AL, Ling Y, Yates PR: The ETS-domain transcription factor family. *Int J Biochem Cell Biol* 29: 1371–1387, 1997
16. Wasylyk B, Hahn SL, Giovane A: The Ets family of transcription factors. *Eur J Biochem* 211: 7–18, 1993
17. Ito M, Nakayama T, Naito S, Matsuu M, Shichijo K, Sekine I: Expression of Ets-1 transcription factor in relation to angiogenesis in the healing process of gastric ulcer. *Biochem Biophys Res Commun* 246: 123–127, 1998
18. Kola I, Brookes S, Green AR, Garber R, Tymms M, Papas TS, Seth A: The Ets-1 transcription factor is widely expressed during murine embryo development and is associated with mesodermal cells involved in morphogenetic processes such as organ formation. *Proc Natl Acad Sci U S A* 90: 7588–7592, 1993
19. Hultgardh NA, Cercek B, Wang JW, Naito S, Lovdahl C, Sharifi B, Forrester JS, Fagin JA: Regulated expression of the ets-1 transcription factor in vascular smooth muscle cells in vivo and in vitro. *Circ Res* 78: 589–595, 1996
20. Naito S, Shimizu S, Maeda S, Wang J, Paul R, Fagin JA: Ets-1 is an early response gene activated by ET-1 and PDGF-BB in vascular smooth muscle cells. *Am J Physiol* 274: C472–C480, 1998
21. Maroulakou IG, Bowe DB: Expression and function of Ets transcription factors in mammalian development: A regulatory network. *Oncogene* 19: 6432–6442, 2000
22. Maroulakou IG, Papas TS, Green JE: Differential expression of ets-1 and ets-2 proto-oncogenes during murine embryogenesis. *Oncogene* 9: 1551–1565, 1994
23. Naito T, Razzaque MS, Nazneen A, Liu D, Nihei H, Koji T, Taguchi T: Renal expression of the Ets-1 proto-oncogene during progression of rat crescentic glomerulonephritis. *J Am Soc Nephrol* 11: 2243–2255, 2000
24. Reisdorff J, En-nia A, Stefanidis I, Floege J, Lovett DH, Mertens PR: Transcriptional factor Ets-1 regulates gelatinase A gene expression in mesangial cells. *J Am Soc Nephrol* 13: 1568–1578, 2002
25. Imgrund M, Grone E, Grone HJ, Kretzler M, Holzman L, Schlondorff D, Rothenpieler UW: Re-expression of the developmental gene Pax-2 during experimental acute tubular necrosis in mice. *Kidney Int* 56: 1423–1431, 1999
26. Terada Y, Tanaka H, Okado T, Shimamura H, Inoshita S, Kuwahara M, Sasaki S: Expression and function of the developmental gene Wnt-4 during experimental acute renal failure in rats. *J Am Soc Nephrol* 14: 1223–1233, 2003
27. Oikawa M, Abe M, Kurosawa H, Hida W, Shirato K, Sato Y: Hypoxia induces transcription factor ETS-1 via the activity of hypoxia-inducible factor-1. *Biochem Biophys Res Commun* 289: 39–43, 2001
28. Raouf A, Li V, Kola I, Watson DK, Seth A: The Ets1 proto-oncogene is upregulated by retinoic acid: Characterization of a functional retinoic acid response element in the Ets1 promoter. *Oncogene* 19: 1969–1974, 2000
29. Solomon DL, Philipp A, Land H, Eilers M: Expression of cyclin D1 mRNA is not upregulated by Myc in rat fibroblasts. *Oncogene* 11: 1893–1897, 1995
30. Tanaka T, Hanafusa N, Ingelfinger JR, Ohse T, Fujuta T, Nangaku M: Hypoxia induces apoptosis in SV40-immortalized rat proximal tubular cells through the mitochondrial pathways, devoid of HIF1-mediated upregulation of Bax. *Biochem Biophys Res Commun* 309: 222–231, 2003
31. Halterman MW, Miller CC, Federoff HJ: Hypoxia-inducible factor-1a mediates hypoxia-induced delayed neuronal death that involves p53. *J Neurosci* 19: 6818–6824, 1999
32. Teruyama K, Abe M, Nakano T, Iwasaka YC, Takahashi S, Yamada S, Sato Y: Role of transcription factor Ets-1 in the apoptosis of human vascular endothelial cells. *J Cell Physiol* 188: 243–252, 2001
33. Terada Y, Inoshita S, Hanada S, Shimamura H, Kuwahara M, Ogawa W, Kasuga M, Sasaki S, Marumo F: Hyperosmolality activates Akt and regulates apoptosis in renal tubular cells. *Kidney Int* 60: 553–567, 2001
34. Terada Y, Okado T, Inoshita S, Hanada S, Kuwahara M, Sasaki S, Yamamoto T, Marumo F: Glucocorticoids stimulate $p21^{CIP1}$ and arrest cell cycle in vitro and in anti-GBM glomerulonephritis. *Kidney Int* 59: 1706–1716, 2001
35. Denker BM, Smith BL, Kuhajda FP, Agre P: Identification, purification, and partial characterization of a novel Mr 28,000 integral membrane protein from erythrocytes and renal tubules. *J Biol Chem* 263: 15634–15642, 1988
36. Yamamoto T, Sasaki S: Aquaporins in the kidney: Emerging new aspects. *Kidney Int* 54: 1041–1051, 1998
37. Nielsen S, Agre P: The aquaporin family of water channels in kidney. *Kidney Int* 48: 1057–1068, 1995
38. Terada Y, Tomita K, Homma MK, Nonoguchi H, Yang T, Yamada T, Yuasa Y, Krebs EG, Sasaki S, Marumo F: Sequential activation of Raf-1 kinase, mitogen-activated protein (MAP) kinase kinase, MAP kinase, and S6 kinase by hyperosmolality in renal cells. *J Biol Chem* 269: 31296–31301, 1994
39. Okado T, Terada Y, Tanaka H, Inoshita S, Nakao A, Sasaki S: Smad7 mediates transforming growth factor-β-induced apoptosis in mesangial cells. *Kidney Int* 62: 1178–1186, 2002
40. Terada Y, Tomita K, Nonoguchi H, Yang T, Marumo F: Different localization and regulation of two types of vasopressin receptor messenger RNA in microdissected rat nephron segments using reverse transcription polymerase chain reaction. *J Clin Invest* 92: 2339–2345, 1993
41. Fort P, Marty L, Piechaczyk M, El SS, Dani C, Jeanteur P, Blanchard JM: Various rat adult tissues express only one major mRNA species from the glyceraldehyde-3-phosphate-dehydrogenase multigenic family. *Nucleic Acids Res* 13: 1431–1442, 1985
42. Gibson UE, Heid CA, Williams PM: A novel method for real time quantitative RT-PCR. *Genome Res* 6: 995–1001, 1996

43. Heid CA, Stevens J, Livak KJ, Williams PM: Real time quantitative PCR. *Genome Res* 6: 986–994, 1996
44. Terada Y, Yamada T, Nakashima O, Tamamori M, Ito H, Sasaki S, Marumo F: Overexpression of cell cycle inhibitors (p16INK4 and p21Cip1) and cyclin D1 using adenovirus vectors regulates proliferation of rat mesangial cells. *J Am Soc Nephrol* 8: 51–60, 1997
45. Bacallao R, Fine LG: Molecular events in the organization of renal tubular epithelium: From nephrogenesis to regeneration. *Am J Physiol* 257: F913–F924, 1989
46. Albanese C, Johnson J, Watanabe G, Eklund N, Vu D, Arnold A, Pestell RG: Transforming p21ras mutants and c-Ets-2 activate the cyclin D1 promoter through distinguishable regions. *J Biol Chem* 270: 23589–23597, 1995
47. Shimizu A, Yamanaka N: Apoptosis and cell desquamation in repair process of ischemic tubular necrosis. *Virchows Arch B Cell Pathol Incl Mol Pathol* 64: 171–180, 1993
48. Ueda N, Kaushal GP, Shah SV: Apoptotic mechanisms in acute renal failure. *Am J Med* 108: 403–415, 2000

Nephrol Dial Transplant (2004) 19: 812–816
DOI: 10.1093/ndt/gfh064

Nephrology
Dialysis
Transplantation

Original Article

Direct transfer of hepatocyte growth factor gene into kidney suppresses cyclosporin A nephrotoxicity in rats

Koji Yazawa[1], Yoshitaka Isaka[2], Shiro Takahara[1], Enyu Imai[2], Naotsugu Ichimaru[1], Yi Shi[1], Yukiomi Namba[1] and Akihiko Okuyama[1]

[1]Department of Urology and [2]Department of Internal Medicine and Therapeutics, Osaka University Graduate School of Medicine, Suita, Japan

Abstract

Background. The clinical utility of cyclosporin A (CsA) has been limited by its nephrotoxicity, which is characterized by tubular atrophy, interstitial fibrosis and progressive renal impairment. Hepatocyte growth factor (HGF), which plays diverse roles in the regeneration of the kidney following acute renal failure, has been reported to protect against and salvage renal injury by acting as a renotropic and anti-fibrotic factor. Here, we investigated protective effects of HGF gene therapy on CsA-induced nephrotoxicity by using an electroporation-mediated gene transfer method.

Methods. CsA was orally administered as a daily dose of 30 mg/kg in male Sprague–Dawley rats receiving a low sodium diet (0.03% sodium). Plasmid vector encoding HGF (200 μg) was transferred into the kidney by electroporation.

Results. HGF gene transfer resulted in significant increases in plasma HGF levels. Morphological assessment revealed that HGF gene transfer reduced CsA-induced initial tubular injury and inhibited interstitial infiltration of ED-1-positive macrophages. In addition, northern blot analysis demonstrated that cortical mRNA levels of TGF-β and type I collagen were suppressed in the HGF group. Finally, HGF gene transfer significantly reduced striped interstitial phenotypic alterations and fibrosis in CsA-treated rats, as assessed by α-smooth muscle actin expression and Masson's trichrome staining.

Conclusions. These results suggest that HGF may prevent CsA-induced tubulointerstitial fibrosis, indicating that HGF gene transfer may provide a potential strategy for preventing renal fibrosis.

Correspondence and offprint requests to: Dr Yoshitaka Isaka, Department of Internal Medicine and Therapeutics, Osaka University Graduate School of Medicine, Suita 565-0871, Japan. Email: isaka@medone.med.osaka-u.ac.jp

Keywords: acute renal failure; cyclosporin A; hepatocyte growth factor gene; kidney; nephrotoxicity

Introduction

The introduction of cyclosporin A (CsA) into clinical practice has resulted in marked improvement in the short-term outcome of organ transplantation, including significant extension in the 1 year survival of renal allografts [1]. However, CsA-induced nephrotoxicity results in long-term graft loss, which limits the clinical utility of this drug. Nephrotoxicity caused by CsA is characterized by tubular atrophy, interstitial fibrosis, hyalinosis of the afferent arteriole and progressive renal impairment [2,3]. Recent studies have shown that CsA-induced nephrotoxicity is associated with an up-regulation of transforming growth factor-β1 (TGF-β1) in type I collagen, and that TGF-β1 is important for the progression of the nephrotoxicity.

Hepatocyte growth factor (HGF), a multifunctional polypeptide originally characterized as a potent mitogen for mature hepatocytes, plays an important role in renal development and in the maintenance of normal adult kidney structure. HGF functions as a potent mitogenic, motogenic, morphogenic and anti-apoptotic factor in renal tubular epithelial cells [4]. Recent studies have suggested that both endogenous and exogenous HGF are protective against the onset and progression of chronic renal diseases in a variety of animal models. Treatment with exogenous HGF protein effectively suppressed phenotypic changes into myofibroblasts, and thus attenuated ECM deposition and interstitial fibrosis by inhibiting TGF-β1 and its receptor expression *in vivo* [5]. These findings suggest HGF may be a candidate for prevention of CsA-induced nephrotoxicity.

Because HGF is rapidly cleared by the liver causing a reduction in its activity [6], intravenous injections exert

only short-term actions on target organs and do not produce continuous effects. Recently, we developed a new gene transfer system for electroporation *in vivo*. We infused DNA solutions via renal artery followed by electric pulses using a tweezers type of electrode to introduce genes into mesangial cells in nearly all of the glomeruli [7]. The electroporation process is free from oncogenicity, immunogenicity and cytotoxicity from viral vectors. We have shown that this electroporation-mediated gene transfer technique produced significantly higher transfection efficiency than the HVJ liposome method [7]. In addition, kidney-targeted gene transfer methods may concentrate actions on the kidney without causing systemic effect. In the present study, we investigated the effects of HGF gene transfer on CsA-induced nephrotoxicity in rat.

Materials and methods

Experimental design

Six-week-old male Sprague–Dawley rats (SLC Japan, Hamamatsu, Japan), weighing 180–190 g on a low-salt diet (0.03% sodium; Test Diet, Richmond, IN, USA) received daily oral doses of CsA at 30 mg/kg (Neoral, Novartis, Japan). In all the following procedures, rats were anaesthetized with pentobarbital. On day 0, the left kidney and renal artery were surgically exposed by a mid-line incision, and a 24-gauge catheter (Terumo, Tokyo, Japan) was inserted into the left renal artery. After clamping the proximal site of the abdominal aorta, the kidney was perfused with PBS via the renal artery, and HGF plasmid DNA (200 μg in 1 ml of PBS) was then injected into the left kidney using a single shot while clamping the renal vein. The kidney was sandwiched with a tweezers-type oval-shaped stainless electrode, and electric pulses were delivered using an electric pulse generator (CUY-21; NEPA GENE, Chiba, Japan). The pulses were square waves and the voltage (75 V) was held constant during the pulse duration. Three pulses of the indicated voltage followed by three additional pulses of the opposite polarity were administrated to the kidney. Intra-pulse delay was 1 s and the duration of the pulse was fixed at 100 ms. In separate groups of rats ($n=6$ per group) on days 7, 14 and 21, plasma samples were collected and kidneys were removed following perfusion with 20 ml of cold PBS from the aorta. CsA-treated rats with sham operations were also used as untreated disease controls (six animals in each group). In all animals, the cortex was carefully dissected from the medulla and was then processed for evaluation by light microscopy, RNA analysis and immunohistochemistry.

Analysis of plasma samples

Blood samples were collected from the aorta into plastic syringes, transferred to metal-free tubes containing potassium-ethylenediaminetetraacetic acid (EDTA), and then chilled on ice. The samples were immediately centrifuged at 4*g* and plasma was stored at −80°C until further determination. Plasma HGF concentration was measured by the enzyme immunogen assay method (Institute of Immunology, Japan).

Morphology

Tissue samples were fixed in 4% buffered paraformaldehyde for 12 h and embedded in paraffin. Samples were cut at 2–4 μm thickness and stained with periodic acid-Schiff (PAS) and Masson's trichrome. Interstitial fibrosis was stained blue with Masson's trichrome and the sections were quantified by a colour image analyser. We selected at random 10 non-overlapping fields from the cortical region for analysis. The fibrotic area relative to the total area of the field was calculated as a percentage by a computer-aided manipulator. Glomeruli and large vessels were not included in the microscopic fields for image analysis. Scores from 10 fields per kidney were averaged, and mean scores from six separate animals per group were then averaged.

Immunohistochemical stainings

Renal tissues were fixed in cold methyl Carnoy's solution for 6 h, placed in 70% ethanol, and then embedded in paraffin. Tissue sections were cut at 4 μm thickness and were dewaxed and stained with anti-rat ED-1 antibody to identify macrophage infiltraton, followed by a second reaction with biotin-labelled anti-rat IgG goat IgG (Vector, Builingame, CA, USA). Finally, an avidin-biotin coupling reaction was performed on the sections (Vectastain Elite; Vector). To identify myofibroblasts, we used monoclonal IgG against human α-smooth muscle actin (SMαA) (EPOS System; Dako). The SMαA-positive area relative to the total area of the field was calculated as a percentage by a computer-aided manipulator. Glomeruli and large vessels were not included in the microscopic fields for image analysis. The scores of 10 fields per kidney were averaged, and mean scores from six separate animals per group were then averaged.

Northern blot analysis

Renal tissue was finely minced with an autoclaved cutter, was immediately immersed in liquid nitrogen, and then homogenized in TRIzol reagent (Gibco BRL, Grand Island, NY, USA). RNA extraction was performed according to manufacturer instructions. After resuspension in Tris–EDTA buffer, 15 μg of RNA were electrophoresed in each lane in 1% agarose gels containing 2.2 M formaldehyde and 0.2 M MOPS (pH 7.0), and transferred to a nylon membrane (Hybond N). The membranes were prehybridized for 1 h at 42°C with 50% formamide, 10% Denhardt's solution, 0.1% sodium phosphate, 5× standard saline citrate (SSC) and 180 mg/ml denatured salmon sperm DNA. They were hybridized overnight at 42°C with cDNA probes labelled with [^{32}P]dCTP by random oligonucleotide priming (RediPrime). The blots were washed twice in 2× SSC, 0.1% SDS at room temperature for 15 min each, and twice in 0.2× SSC, 0.1% SDS at 60°C for 10 min each. Films were exposed at −80°C for ~24 h. Autoradiographs were scanned on an imaging densitometer. The density of bands for glyceraldehydes-3-phosphate dehydrogenase (GAPDH) mRNA was used to control for differences in the total amount of RNA loaded onto each gel line.

Statistical analysis

All values are expressed as means ± SD. Statistical significance, defined as $P<0.01$, was evaluated using one-way analysis of variance.

Results

Physiological studies

Plasma concentrations of HGF were measured by the ELIZA method. In normal control rats, plasma HGF was undetectable (<0.5 ng/ml). CsA treatment increased plasma HGF levels to 48.7±18.8 ng/ml on day 7, which may reflect up-regulation of endogenous HGF following renal injury. Increased plasma HGF levels persisted throughout the experiment (61.1±11.7 and 56.4±24.6 ng/ml at 2 and 3 weeks, respectively). The HGF gene transfer method caused a further increase in plasma HGF levels on day 7 (106.5± 50.5 ng/ml: $P<0.05$ *vs* CsA group). Thereafter, plasma HGF levels declined in HGF-treated rats (67.9±48.5 and 71.3±25.6 ng/ml at 2 and 3 weeks, respectively), but remained higher than in untreated rats.

Light microscopy

PAS staining revealed that CsA treatment induced characteristic histological changes, including tubular atrophy, early striped fibrosis and inflammatory cell infiltration. Importantly, gene transfer of HGF suppressed these tubulointerstitial injuries.

We used Masson's trichrome to cause blue staining of interstitial fibrosis (Figure 1), and used a colour image analyser to semi-quantitatively estimate fibrosis area. The percentage of injured areas per field of cortex was counted at a ×400 magnification in a minimum of 10 fields. In parallel with the tubulointerstitial injury findings, CsA treatment induced progressive fibrosis (5.3±1.2 and 7.2±1.5% at 2 and 3 weeks, respectively), and HGF gene transfer significantly suppressed the development of interstitial fibrosis (3.4±1.2 and 5.2±1.4% at 2 and 3 weeks, respectively; $P<0.01$ *vs* CsA group).

Immunohistochemical staining

The phenotypic transformation into myofibroblasts, estimated by immunohistochemical staining of SMαA, leads to extracellular matrix (ECM) accumulation. There was strong SMαA expression in CsA-treated kidneys (5.5±1.7 % at 3 weeks) with the most pronounced increases around the thickened basement membrane of the Bowman's capsule and degenerated tubules. This strong SMαA expression was inhibited by treatment with the HGF gene transfer method (3.9±1.6%; $P<0.01$ *vs* CsA group) (Figure 2).

In normal control rats, the number of ED-1-positive macrophages was 4.2±1.2 cells per high power field. CsA administration induced marked and continuous infiltration of ED-1-positive macrophages around the damaged tubules and within the interstitium (52.9±17.3 cells per high power field at 3 weeks). The HGF gene transfer procedure decreased this macrophage accumulation (39.2±13.2 cells; $P<0.01$ *vs* CsA group) (Figure 3).

Northern blot

Northern blot analysis was performed on renal cortexes from the three groups. CsA treatment caused an up-regulation of cortical mRNA expression of TGF-β and type I collagen at 3 weeks compared with the normal control group, and HGF treatment reduced the expression of both TGF-β and type I collagen mRNA expression (Figure 4). HGF treatment significantly reduced TGF-β mRNA expression (ratios of TGF-β signal to GAPDH signal: 1.68±0.27 in untreated *vs* 0.81±0.22 in HGF group, $P<0.01$). In parallel with

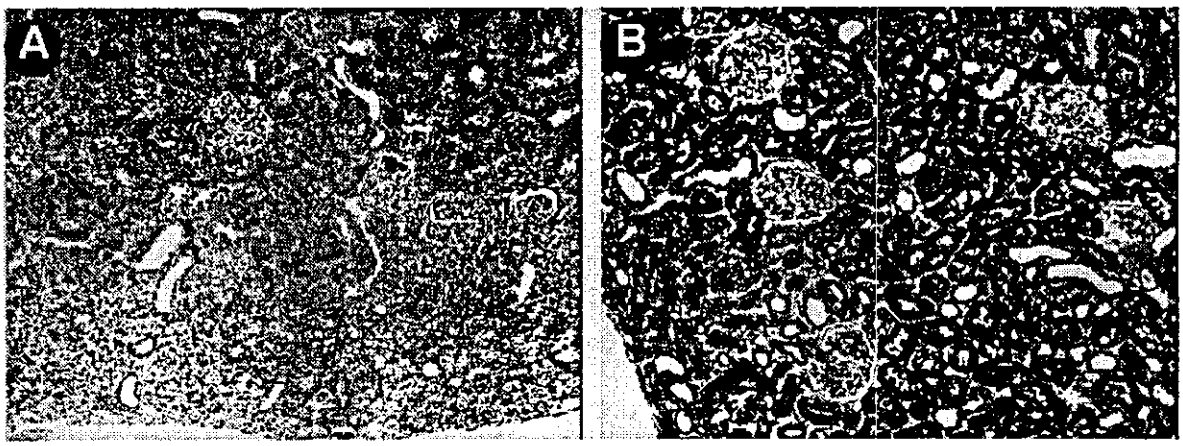

Fig. 1. Representative photomicrographs showing renal morphological changes using Masson's trichrome staining in the CsA (A) and HGF groups (B) at day 21.

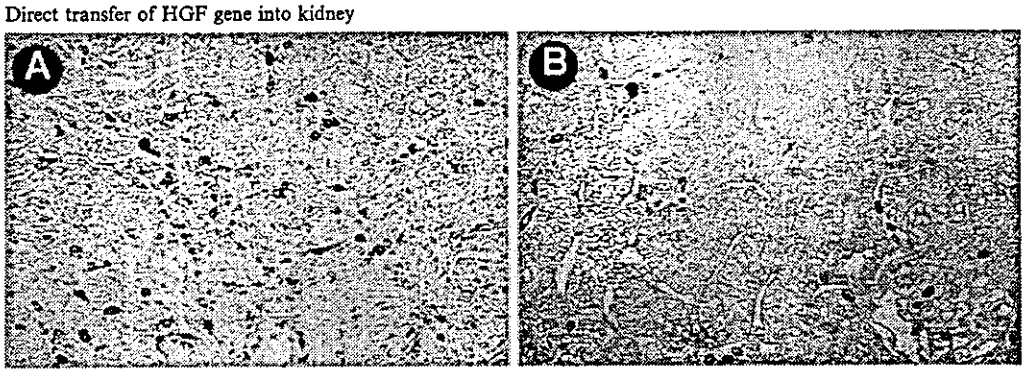

Fig. 2. Representative photomicrographs showing phenotypic changes of interstitium assessed by immunohistochemical staining of SMαA in the CsA (A) and HGF groups (B) at day 21.

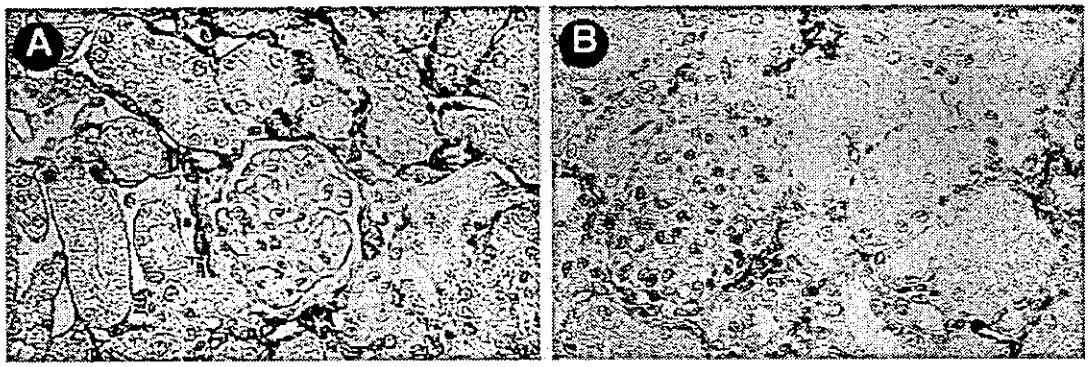

Fig. 3. Representative photomicrographs showing macrophage infiltration into interstitium assessed by immunohistochemical staining of ED-1 in the CsA (A) and HGF groups (B) at day 21.

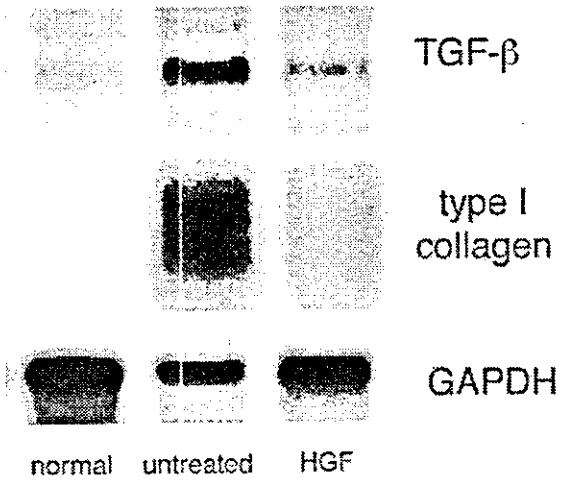

Fig. 4. Northern analysis showing representative cortical mRNA levels of TGF-β (top lane), type I collagen (middle lane) and GAPDH (lower lane) in normal control kidney and in CsA-treated and HGF gene-transferred rats at day 21.

this, type I collagen mRNA was also decreased in HGF-treated kidneys (ratios of type I collagen signal to GAPDH signal: 2.47 ± 0.47 in untreated *vs* 0.69 ± 0.34 in HGF group, $P < 0.001$).

Discussion

In the present study, we found that HGF gene transfer into kidneys using electroporation had a protective effect on chronic CsA-induced nephrotoxicity. Specifically, we demonstrated that HGF gene transfer reduced CsA-induced tubulointerstitial injury, and this included reduced macrophage infiltration, lowered phenotypic alterations of interstitial myofibroblasts and restricted interstitial fibrosis.

Several reports have indicated that HGF is involved in renal regeneration [4]. For example, rapid increases in HGF mRNA and/or protein levels in kidneys and plasma were observed in various types of renal injury induced by nephrotoxins, renal ischaemia and ureteral obstruction [4]. Recently, it was reported that endogenous as well as exogenous HGF prevents renal fibrosis in a mouse model of nephritic syndrome [8]. The present study demonstrated that HGF gene transfection suppressed the expression of TGF-β and reduced interstitial fibrosis.

TGF-β is a fibrotic cytokine and plays an important role in CsA-induced accumulation of ECM protein. The role of TGF-β in mediating CsA nephrotoxicity has been evaluated in several studies. CsA has been shown to up-regulate TGF-β expression in murine tubular cells and tubulointerstitial fibroblasts [9]. In

addition, there is increased TGF-β production in patients with chronic allograft nephropathy and CsA nephrotoxicity [10]. Furthermore, TGF-β antibodies prevent matrix synthesis and attenuate renal injury and renal function in CsA nephrotoxicity [11]. Reciprocal changes in the expressions of TGF-β and HGF were noted during the onset of tubulointerstitial fibrosis caused by unilateral ureter-ligated obstruction in mice [5]. We observed an increase in plasma HGF following CsA treatment (48.7 ± 18.8 ng/ml at day 7), however, continuous renal tissue injury and persistent expression of TGF-β may lead to decreases in endogenous HGF and result in irreversible renal insufficiency. We also found that HGF gene transfer caused further elevations in plasma HGF levels (106.5 ± 50.5 ng/ml), indicating that it may be protective against renal damage at several levels beyond the physiological level. Because HGF is rapidly cleared by the liver which reduces its activity [6], intravenous injections of HGF cause only short-term effects on target organs and do not exert continuous effects. HGF that is expressed in mesangial cells can affect renal cells in a paracrine fashion, especially in tubular cells and in intersitial cells. In addition, HGF gene transfer decreased TGF-β mRNA levels in CsA-treated kidneys. HGF prevents epithelial cell death and the remodelling of renal tissue that occurs with injury or fibrosis, an effect which is opposite to the role of TGF-β. Therefore, exogenous HGF supplementation may prove to be a therapeutic strategy against renal injury. In fact, several studies have demonstrated that HGF has preventive and therapeutic effects in acute and chronic renal failure/renal fibrosis models in laboratory animals. Although it is not known whether HGF causes a direct or indirect suppression of TGF-β expression, this treatment clearly suppresses TGF-β expression and enhances remodelling of renal tissues. These results support the hypothesis that a counterbalance between TGF-β and HGF plays a determinant role in the pathogenesis and therapeutics of fibrosis-related diseases.

Alterations in the phenotype and behaviour of renal fibroblasts may be one of the most important events during the development of interstitial fibrosis. The enhanced expression of SMαA provides a marker of interstitial phenotypic changes, and increased numbers of activated fibroblasts, which are called myofibroblasts and have features of both fibroblasts and smooth muscle cells, accompanies interstitial matrix accumulation. We assessed SMαA expression by immunohistochemistry. Immunostaining of SMαA was strong in the interstitial areas of CsA-treated kidneys, however, immunostaining was weak in the HGF gene-transferred kidneys. Although the precise mechanism of how HGF reduced interstitial SMαA expression is unclear, HGF transfection reduced tubular atrophy induced by CsA treatment. Therefore, HGF appears to suppress the epithelial–mesenchymal transition process.

We used the gene transfer approach instead of recombinant proteins for several reasons. First, since the half life of HGF is quite short, recombinant HGF treatment requires very large doses and frequent injections of recombinant protein. In addition, administrations of high-dose HGF protein may cause adverse effects, and finally, recombinant protein is costly. In contrast, gene transfer is simple, safe, cheap and requires less frequent injections. In the present study, we adopted electroporation-mediated gene transfer into glomeruli.

In summary, we demonstrated that HGF gene transfer reduced CsA-induced interstitial fibrosis by inhibiting TGF-β expression. We speculate that electroporation-mediated HGF gene transfer may be of value in treating chronic CsA-induced nephrotoxicity.

Conflict of interest statement. None declared.

References

1. Opelz G, Dohler B. Cyclosporine and long-term kidney graft survival. *Transplantation* 2001; 72: 1267–1273
2. Shihab FS. Cyclosporine nephropathy: pathophysiology and clinical impact. *Semin Nephrol* 1996; 16: 536–547
3. Shihab FS, Andoh TF, Tanner AM *et al.* Role of transforming growth factor-beta 1 in experimental chronic cyclosporine nephropathy. *Kidney Int* 1996; 49: 1141–1151
4. Matsumoto K, Nakamura T. Hepatocyte growth factor: renotropic role and potential therapeutics for renal diseases. *Kidney Int* 2001; 59: 2023–2038
5. Mizuno S, Matsumoto K, Nakamura T. Hepatocyte growth factor suppresses interstitial fibrosis in a mouse model of obstructive nephropathy. *Kidney Int* 2001; 59: 1304–1314
6. Liu Y. Hepatocyte growth factor promotes renal epithelial cell survival by dual mechanisms. *Am J Physiol* 1999; 277: F624–F633
7. Tsujie M, Isaka Y, Nakamura H, Imai E, Hori M. Electroporation-mediated gene transfer that targets glomeruli. *J Am Soc Nephrol* 2001; 12: 949–954
8. Mizuno S, Kurosawa T, Matsumoto K *et al.* Hepatocyte growth factor prevents renal fibrosis and dysfunction in a mouse model of chronic renal disease. *J Clin Invest* 1998; 101: 1827–1834
9. Wolf G, Thaiss F, Stahl RA. Cyclosporine stimulates expression of transforming growth factor-beta in renal cells. Possible mechanism of cyclosporines antiproliferative effects. *Transplantation* 1995; 60: 237–241
10. Shihab FS, Yamamoto T, Nast CC *et al.* Transforming growth factor-beta and matrix protein expression in acute and chronic rejection of human renal allografts. *J Am Soc Nephrol* 1995; 6: 286–294
11. Islam M, Burke JF Jr, McGowan TA *et al.* Effect of anti-transforming growth factor-beta antibodies in cyclosporine-induced renal dysfunction. *Kidney Int* 2001; 59: 498–506

Received for publication: 4.7.03
Accepted in revised form: 7.11.03

Original Report: Laboratory Investigation

American Journal of Nephrology

Am J Nephrol 2004;24:188–197
DOI: 10.1159/000076758

Received: September 30, 2003
Accepted: January 4, 2004
Published online: February 12, 2004

Different Type and Localization of CD44 on Surface Membrane of Regenerative Renal Tubular Epithelial Cells in vivo

Yuansheng Xie[a,c] Shinichi Nishi[a] Sachiko Fukase[a] Hiroaki Nakamura[b] Xiangmei Chen[c] Naofumi Imai[a] Minoru Sakatsume[a] Akihiko Saito[a] Mitsuhiro Ueno[a] Ichiei Narita[a] Toshio Yamamoto[b] Fumitake Gejyo[a]

[a]Division of Clinical Nephrology and Rheumatology, Niigata University Graduate School of Medical and Dental Sciences, Niigata, and [b]Department of Oral Morphology, Science of Functional Recovery and Reconstruction, Okayama University Graduate School of Medicine and Dentistry, Okayama, Japan; [c]Kidney Center of PLA, Department of Nephrology, Chinese General Hospital of PLA, Beijing, China

Key Words
Acute tubular necrosis · CD44 · Plasma membrane

Abstract
Background: CD44 is a transmembrane glycoprotein comprising an extracellular domain, a transmembrane domain, and a cytoplasmic tail. Previous studies demonstrated that CD44 was generally restricted to lateral-basal plasma membrane (PM) of epithelial cells, whether it localized on apical PM in vivo has not been clarified. ***Methods:*** In this study, we used a gentamicin-induced acute tubular necrosis (ATN) and spontaneous recovery model in rats and two distinct antibodies, an anti-rat distal extracellular domain (OX49) of standard CD44 (CD44-OX49) and an anti-rat CD44 cytoplasmic tail (CD44CPT), to survey the localization of CD44-OX49 and CD44CPT on the PM in renal tubular epithelial cells in different recovery stages after ATN with immunohistochemistry and immunoelectron-microscopic examinations. ***Results:*** CD44-OX49 was localized not only on the lateral-basal PM in tubular epithelial cells, but also on the apical surface membrane in PCNA-positive newly regenerative tubular epithelial cells in early recovery stages after ATN. However, CD44CPT was only localized on the lateral-basal PM. The immunoelectron-microscopic results showed that CD44-OX49 localization was changed from the apical to lateral to basal surface membrane in renal tubular epithelial cells during the recovery process after ATN, finally disappearing from basal PM when normal polarized epithelial cells formed. ***Conclusions:*** These results suggest that there were two types of CD44 including CD44 without a cytoplasmic tail localizing on the apical surface membrane related to newly regenerative epithelial cells, and CD44 with a cytoplasmic tail localizing on the lateral-basal PM related to establishment of tubular epithelial cell polarity after ATN in vivo.

KARGER
Fax + 41 61 306 12 34
E-Mail karger@karger.ch
www.karger.com

0250–8095/04/0242–0188$21.00/0

Accessible online at:
www.karger.com/ajn

Prof. Fumitake Gejyo
Division of Clinical Nephrology and Rheumatology
Niigata University Graduate School of Medical and Dental Sciences
1-757 Asahimachi-dori, Niigata 951-8510 (Japan)
Tel. +81 25 227 2200, Fax +81 25 227 0775, E-Mail gejyo@med.niigata-u.ac.jp

Introduction

The surface of polarized epithelial cells such as renal tubular epithelial cells is typically divided into two functionally and biochemically distinct, but physically continuous, domains separated by junctional complexes, termed apical and lateral-basal (also known as basolateral) plasma membrane (PM) domains [1]. The apical PM, facing the organ lumen, has a protective role by acting as a barrier between the external and internal environments and contains the necessary transporters for the uptake of small molecules. The lateral-basal PM is involved in cell-cell and cell-matrix adhesion, and also contains biological molecules involved in signal transduction and nutrient uptake [2].

CD44 is a broadly distributed multistructural and multifunctional transmembrane glycoprotein. It has at least 20 multiple isoforms of different molecular sizes (85–230 kD), such as standard CD44 or hemotopietic CD44, variant CD44 and epithelial CD44. The major physiological role of CD44 is to maintain organ and tissue structure via cell-cell and cell-matrix adhesion, while it is also involved in cell motility and migration, differentiation, cell signaling and gene transcription [3]. The CD44 protein is a single chain molecule comprising an N-terminal extracellular domain, a transmembrane domain, and a cytoplasmic tail [4]. The cytoplasmic tail of CD44 contributes to ligand and cytoskeletal associated protein binding, and determines membrane localization in polarized epithelial cells [5, 6]. In vitro studies have demonstrated that in polarized Madin-Darby canine kidney (MDCK) epithelial cell cultures, a tailless CD44 molecule is localized on the apical PM, whereas wild-type CD44 is restricted to the lateral-basal PM of epithelial cells, suggesting that the localization of CD44 may be regulated [7]. However, in vivo studies demonstrated that CD44 is generally localized on the lateral-basal PM of renal tubular polarized epithelial cells [8], and it remains unclear whether CD44 is also localized on the apical PM of tubular epithelial cells in any pathophysiological condition and the structure of CD44 located on distinct surface membrane of tubular epithelial cells in vivo.

Our previous study showed the up-regulated expression of CD44 in renal tubules during the recovery process after acute tubular necrosis (ATN) [9], but the exact localization and distribution of CD44 during the process of injury and repair of the kidneys remains poorly understood. In this study, we used a gentamicin-induced ATN and spontaneous recovery model in rats and two distinct antibodies, an anti-rat distal extracellular domain (OX49) of standard CD44 (CD44-OX49) and an anti-rat CD44 cytoplasmic tail (CD44CPT), surveyed the different localization of CD44-OX49 and CD44CPT in the surface membranes of renal tubular epithelial cells in different recovery stages after ATN and discussed the potential roles of CD44 localized on different surface membrane.

Methods

Animal Examination

Experiments were performed on 32 male Wistar rats (Charles River Japan, Yokohama, Japan) weighing between 220 and 250 g that were divided into two groups: a gentamicin group including 20 rats and a control group including 12 rats. The rats in the gentamicin group were given 150 mg/kg/day of gentamicin sulphate solution (Sigma-Aldrich Co. St. Louis, Mo., USA) by subcutaneous injection in the neck for 5 days, and the rats in the control group were given an equal volume of normal saline instead. All animals were fed a diet of standard laboratory chow and allowed free access to water, but were deprived of water for 24 hours before the first gentamicin administration, and for 12 hours a day during gentamicin administration. Five rats in the gentamicin group and 3 rats in the control group were sacrificed under ether anesthesia on days 6, 10, 15, and 30 after the first gentamicin injection, respectively. The left kidney of each rat was removed and bisected for routine histological examination by general light microscopy and general electron microscopy. Then, each rat was infused with 4% paraformaldehyde from the abdominal aorta and the right kidney was removed and bisected for immunohistochemical and immunoelectron-microscopic examination.

Primary Antibodies

The following primary antibodies were used in this study: a purified mouse anti-rat CD44H (also known as CD44s; clone: OX-49, a distal extracellular domain of standard CD44, named as CD44-OX49 by the author) monoclonal antibody (PharMingen, San Diego, Calif., USA), a purified rabbit anti-rat CD44 cytoplasmic tail (CD44CPT) antibody (see below) and a mouse anti-proliferating cell nuclear antigen (PCNA) monoclonal antibody (Dako, Glostrup, Denmark).

According to a previous report, residues 423–503 of rat CD44 were located in the cytoplasmic region [10]. An antibody against rat CD44CPT was constructed using the following procedure. A cysteine-conjugated peptide corresponding to residues 483–503 (DQFMTADETRNLQSVDMKIGV) of rat CD44 was synthesized and coupled via a terminal cysteine residue to keyhole limpet hemocyanin. This antigen was subcutaneously injected into rabbits and antisera were collected. A specific antibody to CD44CPT was purified with Affi-Gel 10 (Bio-Rad, Hercules, Calif., USA) coupled with the peptide. The antibody test for CD44CPT showed that the antibody prepared against CD44CPT was stable and special in its activity to CD44CPT.

The antibodies against rat CD44-OX49 and CD44CPT needed not any special antigen retrieval techniques in their use.

Immunohistochemistry

Immunohistochemical staining was carried out on 3-μm wax sections. The sections were first dewaxed and dehydrated. Then, they

were incubated with 0.6% H_2O_2 in methanol for 30 min to eliminate endogenous peroxidase activity and incubated with normal goat serum (Chemicon, Temecula, Calif., USA) at room temperature for 30 min to block non-special reaction. Subsequently, they were incubated at 4°C for 24 h with primary antibodies, mouse anti-rat CD44-OX49 (2.5 μg/ml) or rabbit anti-CD44CPT (1.5 μg/ml) or mouse anti-PCNA (1:20). After washing in PBS for 3 × 5 min, the sections were incubated with a secondary antibody (Dako, EnVision+™, Carpinteria, Calif., USA), goat anti-mouse IgG (for CD44-OX49) or goat anti-rabbit IgG (for CD44CPT) conjugated with peroxidase, or goat anti-mouse IgG conjugated with alkaline phosphatase (for PCNA), at room temperature for 30 min. After washing with PBS, the sections were incubated with a DAB peroxidase substrate solution (Nichirei, Tokyo, Japan) or a Fuchsin alkaline phosphatase substrate solution (Dako, Carpinteria, Calif., USA) with an endogenous alkaline phosphatase inhibitor (Dako). The cellular nuclei of the sections were counterstained with hematoxylin. Normal mouse IgG and normal rabbit IgG were used as negative controls, respectively (Santa Cruz Biotechnology, Calif., USA).

Double Staining

Double staining was performed on the same tissue section, which included a combination of CD44-OX49 immunohistochemistry and PCNA immunohistochemistry (see above) as a marker of cell proliferation or regeneration. The first immunostaining for CD44-OX49 was performed with a DAB peroxidase substrate solution, which caused a brown color reaction, followed by washing in PBS for 3 × 5 min and treatment for 10 min in a microwave oven in a 0.01 *M* citrate buffer (pH 6.0). Then, the second immunostaining for PCNA was performed with a Fuchsin alkaline phosphatase substrate solution, which caused a red color reaction.

Immunoelectron-Microscopic Examination

After perfusion fixation with 4% paraformaldehyde, each rat kidney was removed, cut into some small blocks (2 × 2 × 2 mm) and taken into fusion fixated with 4% phosphate buffered paraformaldehyde and 0.01% glutaraldehyde for 2–4 h at 4°C. The tissue was then washed overnight in a 0.1 *M* phosphate buffer (PB), and washed further in graded 10, 15 and 20% sucrose PBS series for 24 h at 4°C, respectively. After rinsing in a mixed solution of 20% sucrose and 8% glycerin PBS for 2 h at 4°C, the tissue was embedded with optimal cutting temperature (OCT) compound in acetone and dry ice ethanol. Approximately 10–20 μm frozen sections were obtained with a frozen microslicer. Then, according to the above immunohistochemical staining procedure, the sections were preincubated with 0.6% H_2O_2 in methanol and normal goat serum for 30 min at room temperature, respectively, and incubated with a purified mouse anti-rat CD44-OX49 monoclonal antibody (2.5 μg/ml) for 24 h at 4°C, followed by a goat anti-mouse second antibody conjugated with peroxidase for 30 min. After washing with PBS, the sections were incubated with a DAB peroxidase substrate solution. After postfixation with 2% osmium tetroxide (OsO_4) in 0.1 *M* PB for 2 h, the specimens were dehydrated in a graded 50, 60, 70, 80, 90 and 100% (three times) ethanol series for 10 min, respectively, embedded in epoxy resin (Epok 812; Oken, Tokyo, Japan) and polymerized at 60°C for 5 days. Ultrathin sections with 90–100 nm were obtained and half of the sections were stained with lead citrate for 3 min and observed under a H-7100 transmission electron microscope (Hitachi, Tokyo, Japan) at an accelerating voltage of 75 kV.

Quantitative Analysis

Quantitative analysis was performed to investigate the distribution of CD44 on epithelial cell PM in distinct stages in gentamicin-induced ATN and its recovery process. Observations were performed on 100 non-overlapping random tubules 20 per rat kidney section from 5 rats at days 6, 10, 15 and 30 after the first gentamicin administration. Day 6, 100 totally necrotic tubules stained with CD44-OX49; day 10, 100 tubules with PCNA positive staining – these tubules were stained using the double staining technique PCNA and CD44-OX49; day 15 and day 30, 100 tubules with CD44-OX49 positive staining. The number of CD44-OX49-positive stained tubules with stained cells greater than 50% of PM was recorded. If both the basolateral PM and the apical PM were stained in greater than 50% cells these were recorded separately as basolateral PM positive and apical PM positive. If the tubules were not fully necrotic in tubules on day 6, tubules which were PCNA-negative on day 10 or tubules with less than 50% cells stained for CD44-OX49 were not recorded as positive tubules.

Results

Histopathological Findings

As described previously [9], renal proximal tubular necrosis appeared to develop on day 6 (day 1–5 administration of gentamicin) in the gentamicin group. On day 10, there was a lot of desquamated epithelial cell debris in the dilated tubular lumens. Mononuclear cells infiltrated interstitial regions and tubular lumens from the superficial cortex to the corticomedullary zone. Newly regenerative tubular epithelial cell lines appeared along the tubular

Fig. 1. Localization of distal extracellular domain (OX49) of standard CD44 (CD44-OX49) and CD44 cytoplasmic tail (CD44CPT). Sections labelled **a**, **c**, **e**, and **g** show immunohistochemical staining of CD44-OX49 (brown) and cellular nuclear staining at days 6, 10, 15, and 30 after the first gentamicin administration (150 mg/kg/day × 5), respectively. Serial sections **b**, **d**, **f**, and **h** show immunohistochemical staining of CD44CPT (brown) and cellular nuclear staining at days 6, 10, 15 and 30 after the first gentamicin administration, respectively. On day 6, CD44-OX49 (arrow, **a**) and CD44CPT (arrow, **b**) are negative in the desquamated epithelia, denuded tubular basement membranes. CD44-OX49 and CD44CPT are positive in only non-necrotic tubules. On day 10, CD44-OX49 is markedly positive on the apical plasma membrane (PM) in newly regenerative epithelial cells (arrow, **c**), whereas CD44CPT is negative on the same apical PM (arrow, **d**). On day 15, CD44-OX49 (arrow, **e**) and CD44CPT (arrow, **f**) are almost identically located on the lateral PM. On day 30, CD44-OX49 (arrow, **g**) and CD44CPT (arrow, **h**) are almost identically expressed on the basal PM in non-full recovery tubular epithelial cells, but are negative in normal or full recovery tubular epithelial cells (triangle, **g** and **h**, respectively). Original magnification × 100.

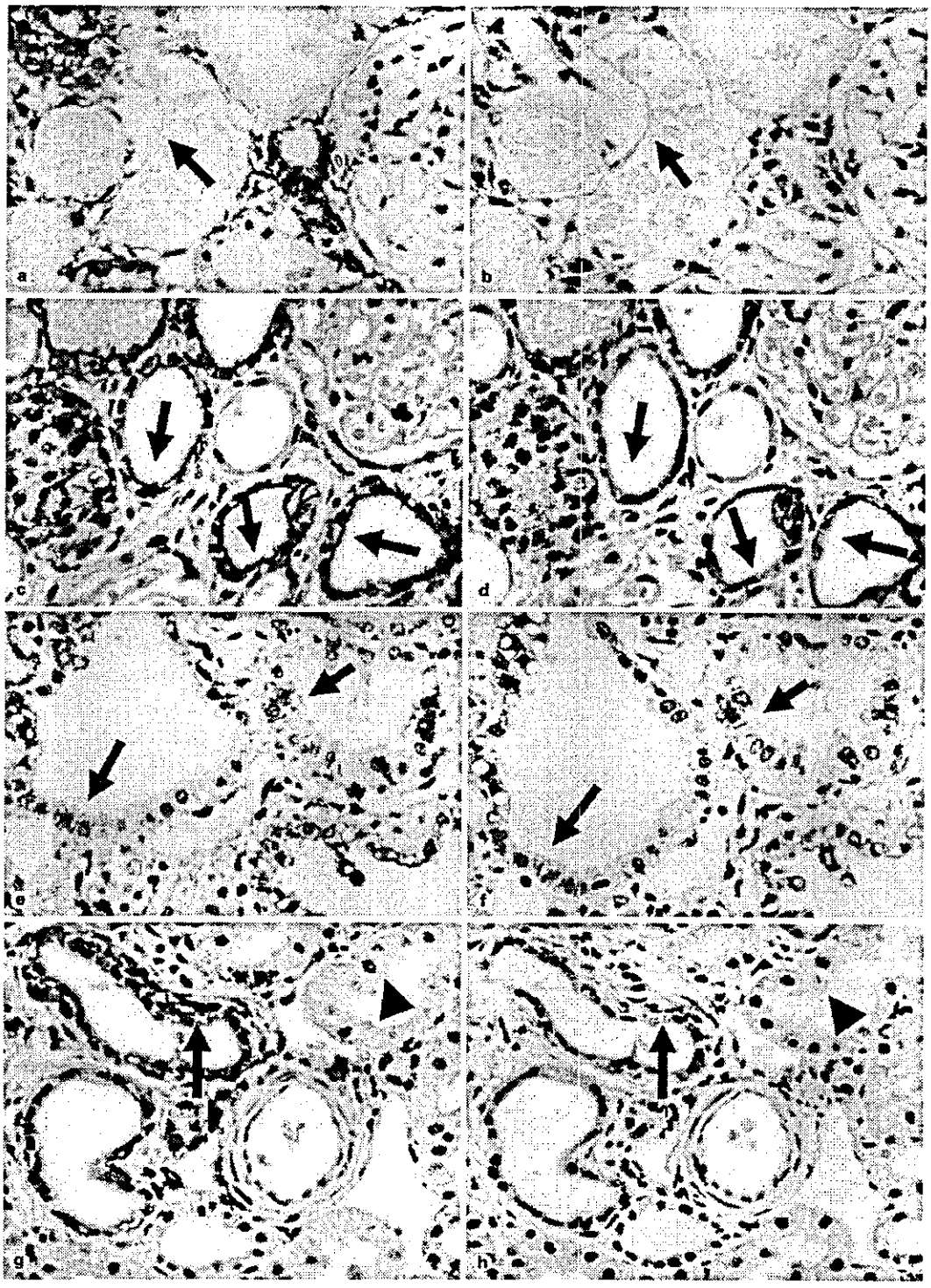
a
b
c
d
e
f
g
h

basement membranes. On day 15, the regenerative tubular epithelial cells became larger and the renal tubular epithelium became thicker. On day 30, most of the cortical tubular structures recovered close to the normal architecture, but spotty infiltration of mononuclear cells, atrophy of renal tubules and fibrosis of the interstitium remained. The control group showed no significant histological changes throughout the experimental period (data not shown).

Apical and Lateral-Basal Localization of CD44-OX49

To determine the localization of CD44-OX49 in rat kidneys after ATN, we performed immunohistochemistry using a purified mouse anti-rat CD44-OX49 monoclonal antibody and counterstaining for cellular nuclei with hematoxylin. In the control group, no expression of CD44-OX49 in the cortical tubular epithelial cells was found throughout the experimental period, except for a few monocytes and Bowman's capsule (data not shown). CD44-OX49 staining was markedly increased in the cortical tubular epithelial cells and infiltrating cells in the cortical interstitium and tubular lumens from the early tubular necrotic period to the later recovery period in the gentamicin group. CD44-OX49 staining was markedly increased at the lateral-basal PM in non-necrotic tubular epithelial cells, whereas it was not found on the denuded basement membrane of full necrotic tubules on day 6 after the first gentamicin administration. CD44-OX49 staining was markedly increased on the apical PM in the regenerative tubular cells on day 10, the lateral PM on day 15 and the basal PM on day 30 in the gentamicin group (fig. 1a, c, e, g). There were no positive findings in negative control samples using normal mouse IgG (data not shown).

Lateral-Basal Localization of the CD44 Cytoplasmic Tail

In order to prove whether CD44 localized on the apical PM was a tailless CD44 or not, we performed immunohistochemical staining using a purified rabbit anti-rat CD44CPT antibody and counterstaining for cellular nuclei with hematoxylin on serial sections. As with CD44-OX49, no expression of CD44CPT in the cortical tubular epithelial cells was found throughout the experimental period in the control group (data not shown). The CD44CPT staining was markedly increased at the lateral-basal PM in the non-necrotic tubular epithelial cells and was not localized on the denuded basement membrane of necrotic tubules on day 6 after the first gentamicin administration. The CD44CPT staining was markedly increased at lateral or lateral-basal PM on days 10 and 15 and on the basal or lateral-basal PM on day 30 in regenerative tubular epithelial cells in the gentamicin group. However, CD44CPT was not found on the apical PM in tubular epithelial cells (fig. 1b, d, f, h). There were no positive findings in negative control samples using normal rabbit IgG (data not shown).

Change of CD44-OX49 Localization on Surface Membrane

In order to clarify the changing process of CD44-OX49 localization from the apical to lateral-basal surface membrane in regenerative tubular epithelial cells after ATN in the gentamicin group, we performed immuno-electron microscopic examination with CD44-OX49. As a result, on day 10 after the first gentamicin administration, CD44-OX49 was mainly expressed on apical surface of the tubular basement membrane or at the newly regenerative complanate epithelial cell apex. In some tubular epithelia, CD44-OX49 was also expressed on the apical and lateral PM. On day 15, CD44-OX49 was mainly localized on the lateral PM and gradually excluded from the apical surface. Tight contact (cell-cell adhesion) between CD44-OX49-positive lateral PM of cells was generally found at that time. On day 30, CD44-OX49 was mainly localized on the basal PM and gradually excluded from the lateral surface. Finally, CD44 disappeared from basal PM when normal polarized epithelial cells formed (fig. 2).

Fig. 2. Change of CD44-OX49 localization from the apical to lateral-basal surface membrane in the recovery process after acute tubular necrosis. Immuno-electron microscopic examination with CD44-OX49 (**a–f**) shows that in the early recovery stage after gentamicin-induced acute tubular necrosis, CD44-OX49 is expressed on the apical surface of the tubular basement membrane (**a**) or at newly regenerative complanate epithelial cell apex (**b**). In some tubular epithelia, CD44-OX49 is expressed on the apical and lateral PM (**c**). In the middle recovery stage, CD44-OX49 is localized on the lateral PM and excluded from the apical surface (**d**). In some tubular epithelia, CD44-OX49 is expressed on the lateral and basal PM (**e**). Note the close contact (cell-cell adhesion) between the CD44-OX49-positive lateral PM of cells (**c**, **d**, **e**, arrow). In the later recovery stage, CD44-OX49 is localized on the basal PM (**f**, arrow). By that time, partial microvilli of epithelial cells have been formed (**f**, triangle). Finally, immunoelectron-microscopic examination with CD44-OX49 and lead citrate for 3 min shows that staining for CD44-OX49 disappears in the lateral and basal PM (**g**, arrow) when microvilli of normal polarized epithelial cells have been formed (**g**, triangle).